Kavli Institute for Theoretical Physics
University of California, Santa Barbara

Quantifying and Understanding the Galaxy — Halo Connection
July 7, 2017

Structural Evolution in the Galaxy-Halo Connection, and Halo Properties as a Function of Environment Density and Web Location

Joel Primack
UCSC

with collaborators including Aldo Rodriguez-Puebla, Christoph Lee, Peter Behroozi, Sandy Faber, Radu Dragomir, Tze Ping Goh, Miguel Aragon Calvo, Doug Hellinger, Anatoly Klypin, Viraj Pandya, Rachel Somerville, & Avishai Dekel

Halo and Subhalo Demographics with Planck Cosmological Parameters: Bolshoi-Planck and MultiDark-Planck Simulations

Aldo Rodrìguez-Puebla, Peter Behroozi, Joel Primack, Anatoly Klypin, Christoph Lee, Doug Hellinger

MNRAS 2016

Cosmological Simulations

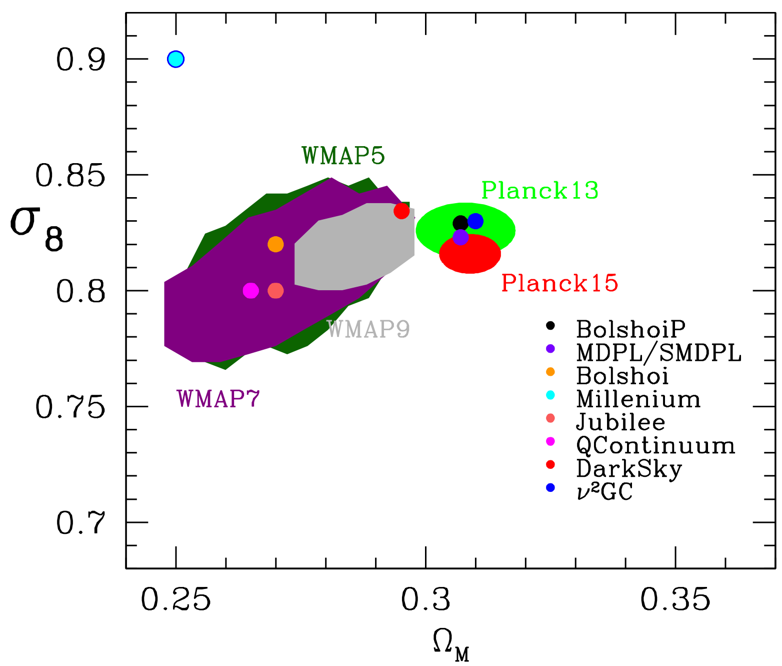

Halo Mass Function and Fits

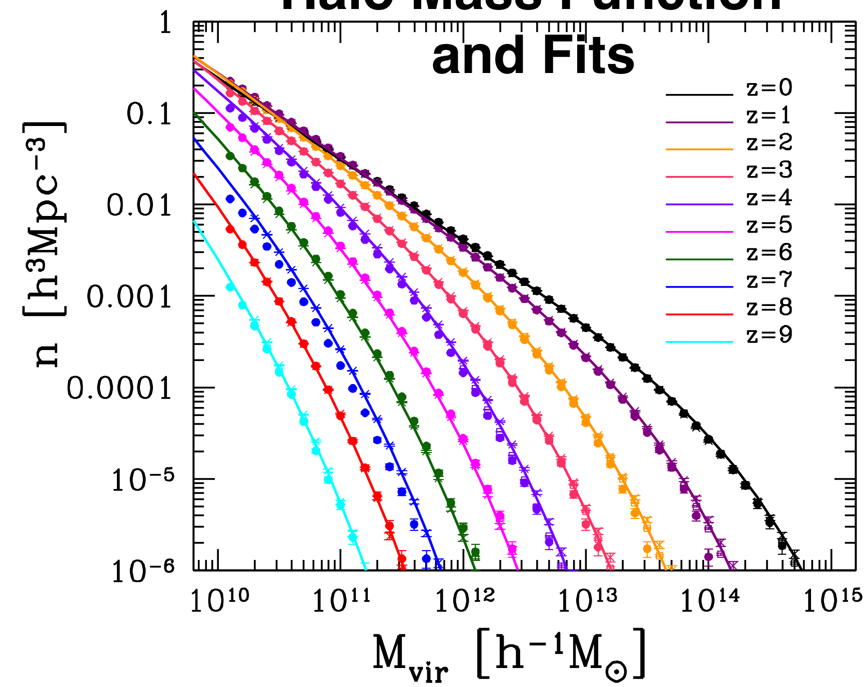

$V_{max}(M_{vir}, z)$

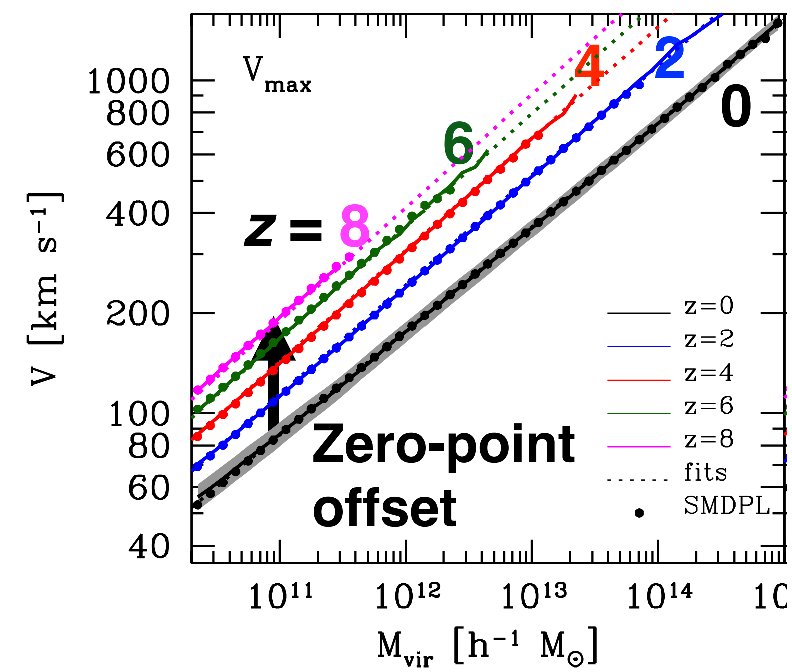

Halo Spin Parameters as a function of M_{vir}

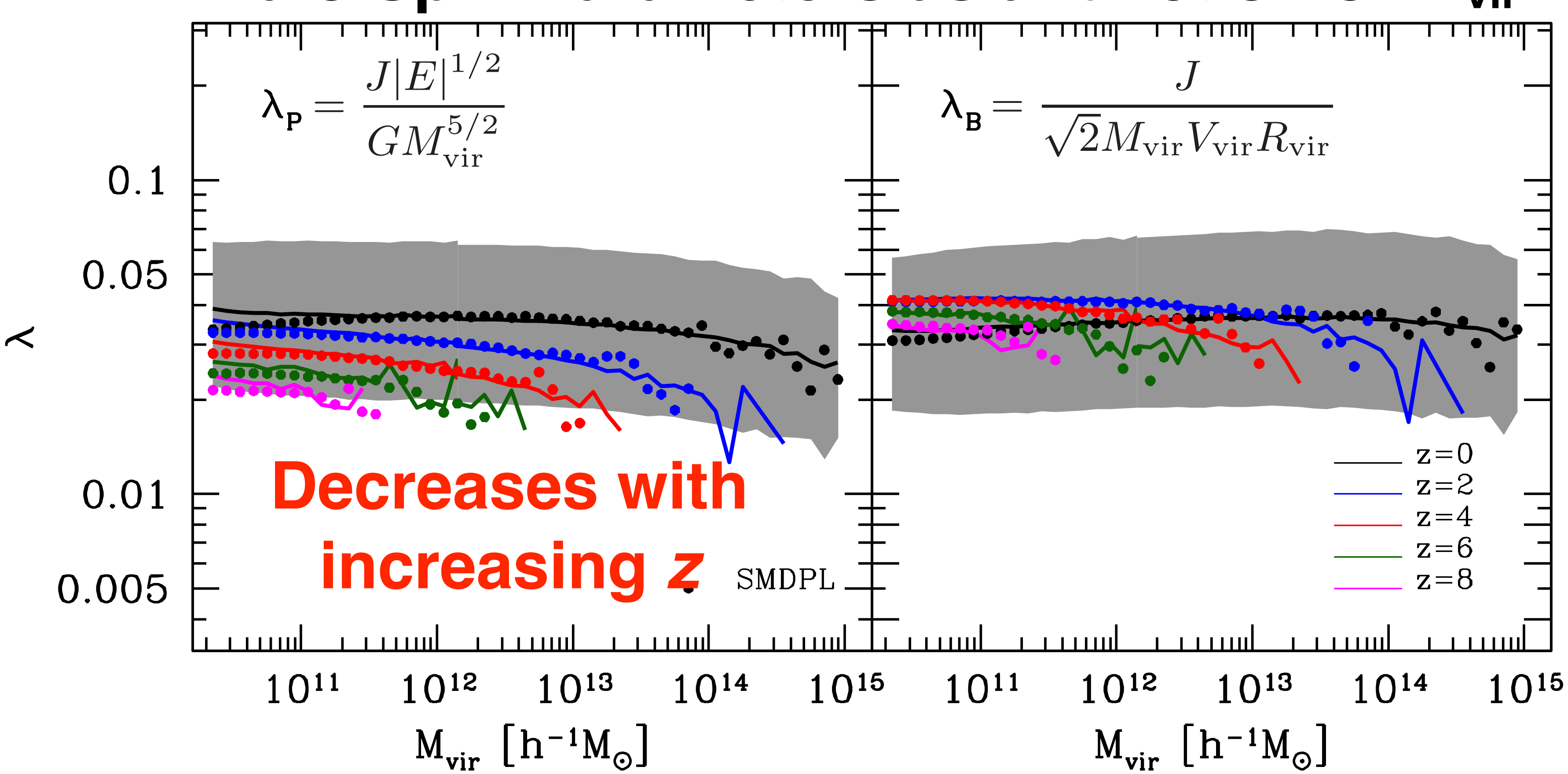

Medians are shown as the solid lines. At z = 0 the grey area is the 68% range.

We have released the halo catalogs and merger trees from Bolshoi-Planck and MultiDark-Planck cosmological simulations. Our paper includes Appendices with instructions for reading these files.

http://hipacc.ucsc.edu/Bolshoi/MergerTrees.html

Constraining the Galaxy Halo Connection: Star Formation Histories, Galaxy Mergers, and Structural Properties

Aldo Rodriguez-Puebla, Joel Primack, Vladimir Avila-Reese, Sandra Faber

MNRAS 2017

Author	Redshift^a	Ω [deg^2]	Corrections
Bell et al. (2003)	$z \sim 0.1$	462	I+SP+C
Yang, Mo & van den Bosch (2009a)	$z \sim 0.1$	4681	I+SP+C
Li & White (2009)	$z \sim 0.1$	6437	I+P+C
Bernardi et al. (2010)	$z \sim 0.1$	4681	I+SP+C
Bernardi et al. (2013)	$z \sim 0.1$	7748	I+SP+C
Rodriguez-Puebla et al. in prep	$z \sim 0.1$	7748	S
Drory et al. (2009)	$0 < z < 1$	1.73	SP+C
Moustakas et al. (2013)	$0 < z < 1$	9	SP+D+C
Pérez-González et al. (2008)	$0.2 < z < 2.5$	0.184	I+SP+D+C
Tomczak et al. (2014)	$0.2 < z < 3$	0.0878	C
Ilbert et al. (2013)	$0.2 < z < 4$	2	C
Muzzin et al. (2013)	$0.2 < z < 4$	1.62	I+C
Santini et al. (2012)	$0.6 < z < 4.5$	0.0319	I+C
Mortlock et al. (2011)	$1 < z < 3.5$	0.0125	I+C
Marchesini et al. (2009)	$1.3 < z < 4$	0.142	I+C
Stark et al. (2009)	$z \sim 6$	0.089	I
Lee et al. (2012)	$3 < z < 7$	0.089	I+SP+C
González et al. (2011)	$4 < z < 7$	0.0778	I+C
Duncan et al. (2014)	$4 < z < 7$	0.0778	C
Song et al. (2015)	$4 < z < 8$	0.0778	I
This paper, Appendix D	$4 < z < 10$	0.0778	–

I=IMF; P= photometry corrections; S=Surface Brightness correction; D=Dust model; NE= Nebular Emissions: SP = SPS Model: C = Cosmology

Author	Redshift^a	SFR Estimator	Corrections	Type
Chen et al. (2009)	$z \sim 0.1$	H_α/H_β	S	All
Salim et al. (2007)	$z \sim 0.1$	UV SED	S	All
Noeske et al. (2007)	$0.2 < z < 1.1$	UV+IR	S	All
Karim et al. (2011)	$0.2 < z < 3$	1.4 GHz	I+S+E	All
Dunne et al. (2009)	$0.45 < z < 2$	1.4 GHz	I+S+E	All
Kajisawa et al. (2010)	$0.5 < z < 3.5$	UV+IR	I	All
Whitaker et al. (2014)	$0.5 < z < 3$	UV+IR	I+S	All
Sobral et al. (2014)	$z \sim 2.23$	H_α	I+S+SP	SF
Reddy et al. (2012)	$2.3 < z < 3.7$	UV+IR	I+S+SP	SF
Magdis et al. (2010)	$z \sim 3$	FUV	I+S+SP	SF
Lee et al. (2011)	$3.3 < z < 4.3$	FUV	I+SP	SF
Lee et al. (2012)	$3.9 < z < 5$	FUV	I+SP	SF
González et al. (2012)	$4 < z < 6$	UV+IR	I+NE	SF
Salmon et al. (2015)	$4 < z < 6$	UV SED	I+NE+E	SF
Bouwens et al. (2011)	$4 < z < 7.2$	FUV	I+S	SF
Duncan et al. (2014)	$4 < z < 7$	UV SED	I+NE	SF
Shim et al. (2011)	$z \sim 4.4$	H_α	I+S+SP	SF
Steinhardt et al. (2014)	$z \sim 5$	UV SED	I+S	SF
González et al. (2010)	$z = 7.2$	UV+IR	I+NE	SF
This paper, Appendix D	$4 < z < 8$	FUV	I+E+NE	SF

I=IMF; S=Star formation calibration; E=Extinction; NE= Nebular Emissions; SP=SPS Model

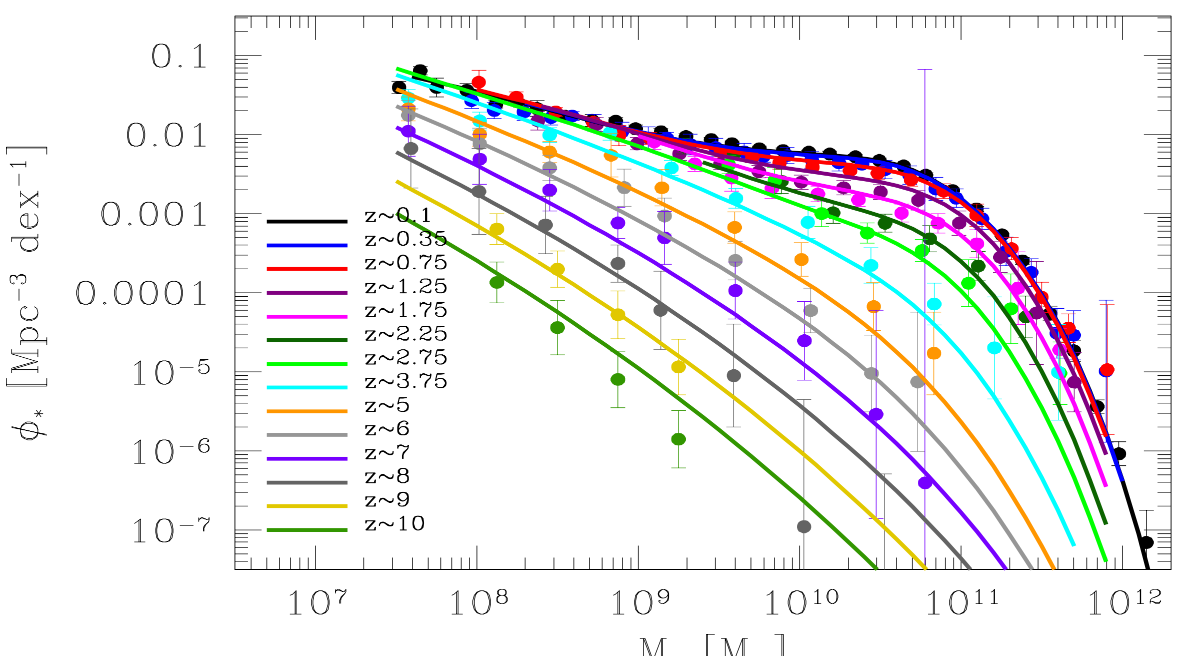

Redshift evolution from z ~ 0.1 to z ~ 10 of the galaxy stellar mass function derived by using 20 observational samples from the literature and represented by filled circles with error bars. The various data has been corrected for potential systematics that could affect our results. Solid lines are the best fit model from a set of 3×10^5 MCMC trials.

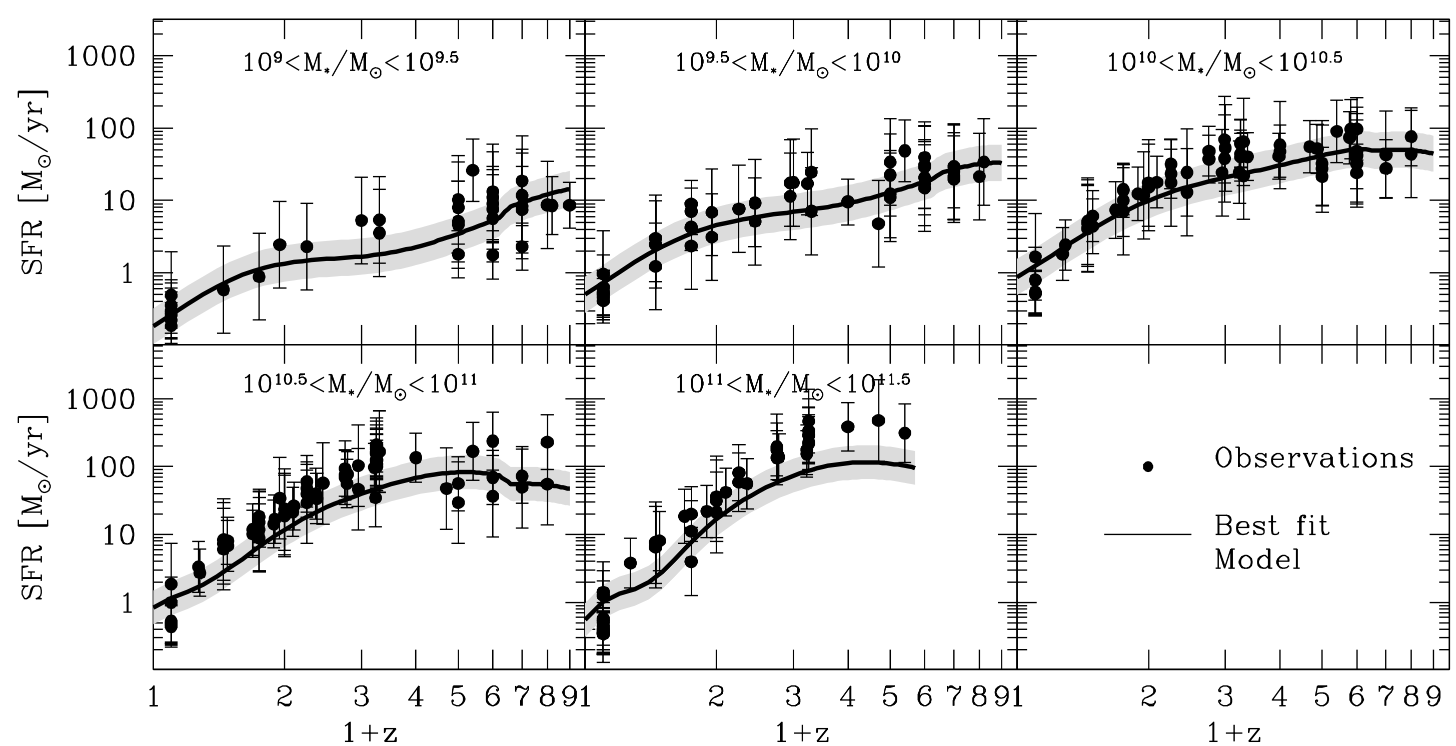

Star formation rates as a function of redshift z in five stellar mass bins. Filled circles with error bars show the observed data. Black solid lines show our best fit model to the SFRs.

Constraining the Galaxy Halo Connection: Star Formation Histories, Galaxy Mergers, and Structural Properties

Aldo Rodriguez-Puebla, Joel Primack, Vladimir Avila-Reese, Sandra Faber

MNRAS 2017

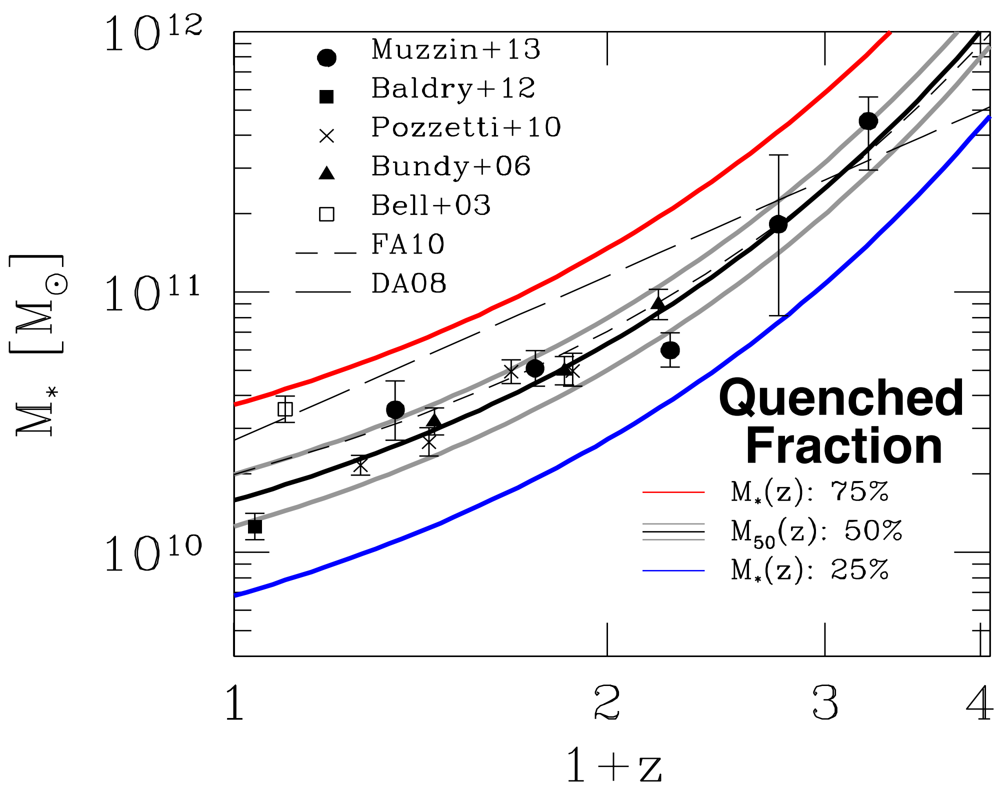

Average Stellar Mass Halo Mass Relation

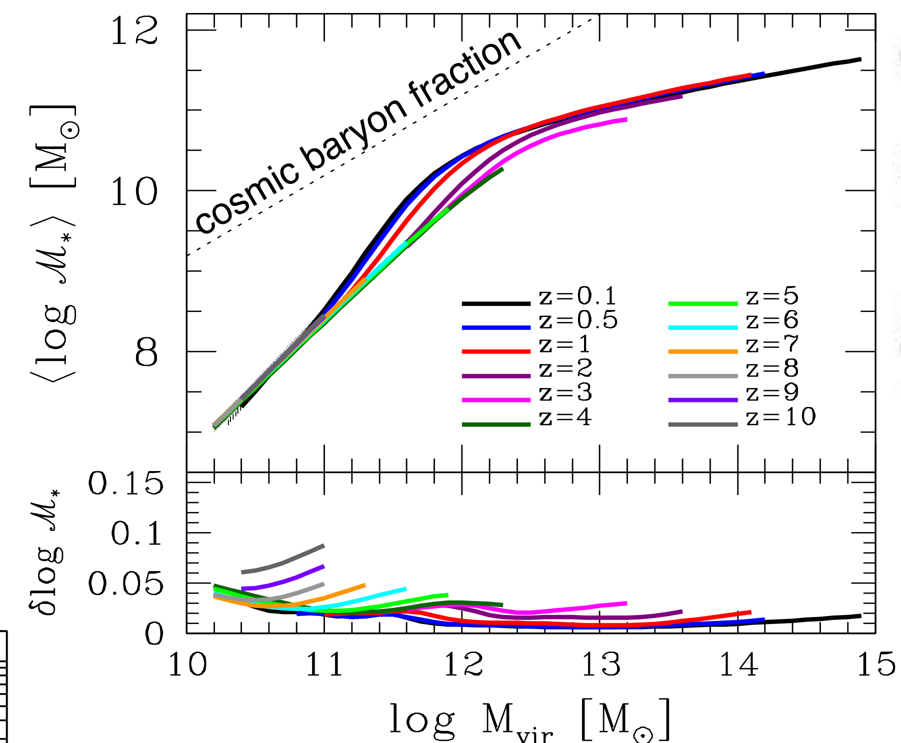

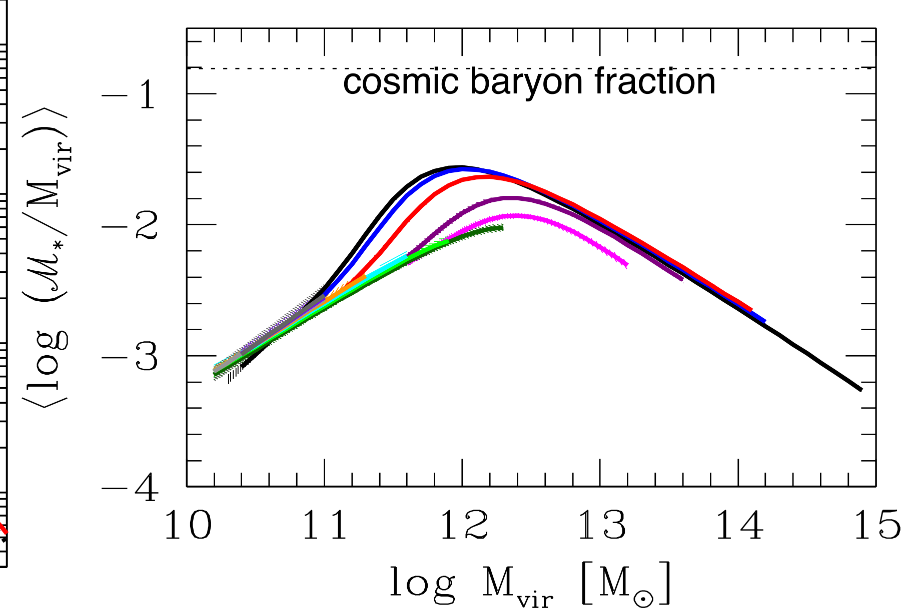

Star Formation Rate Density

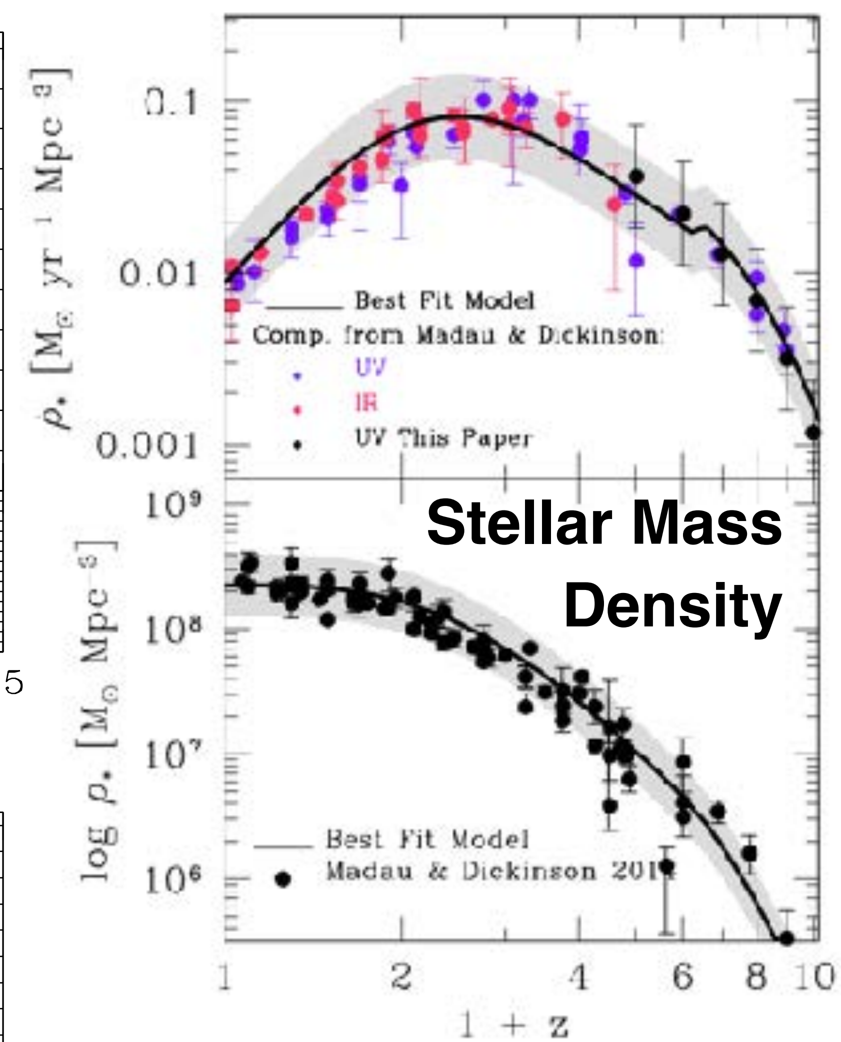

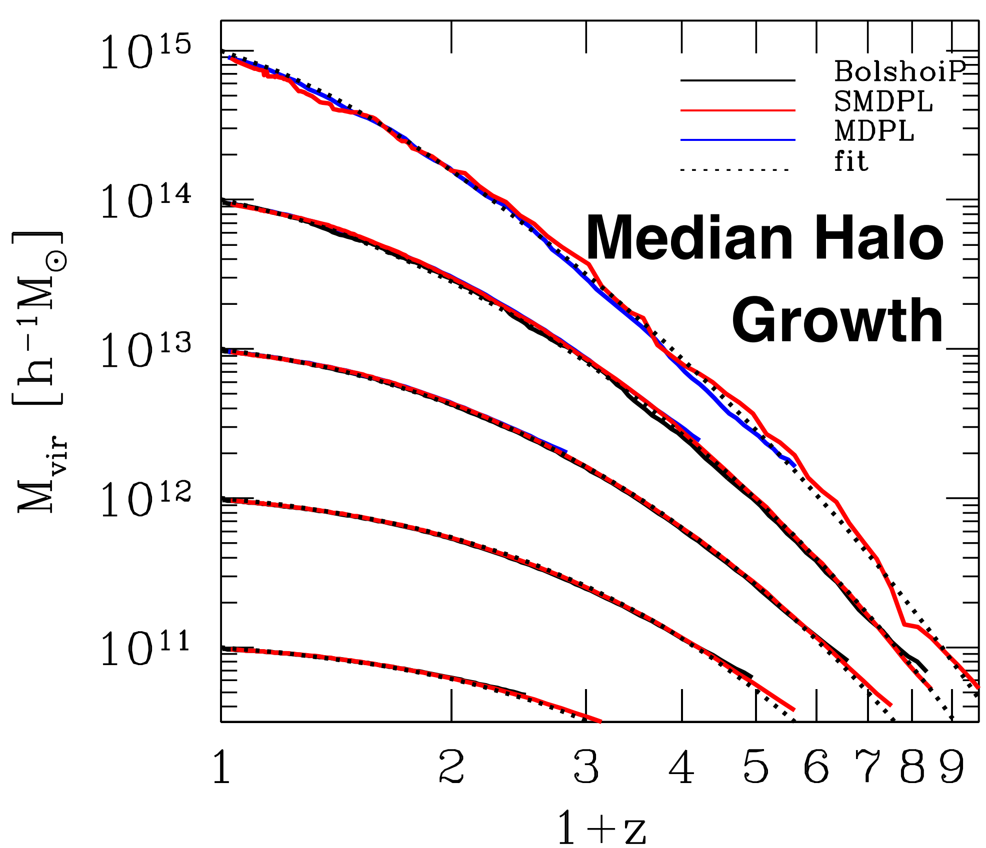

Constraining the Galaxy Halo Connection: Star Formation Histories, Galaxy Mergers, and Structural Properties

Aldo Rodriguez-Puebla, Joel Primack, Vladimir Avila-Reese, Sandra Faber

MNRAS 2017

SFR vs. M*, M_{vir}, and *z*

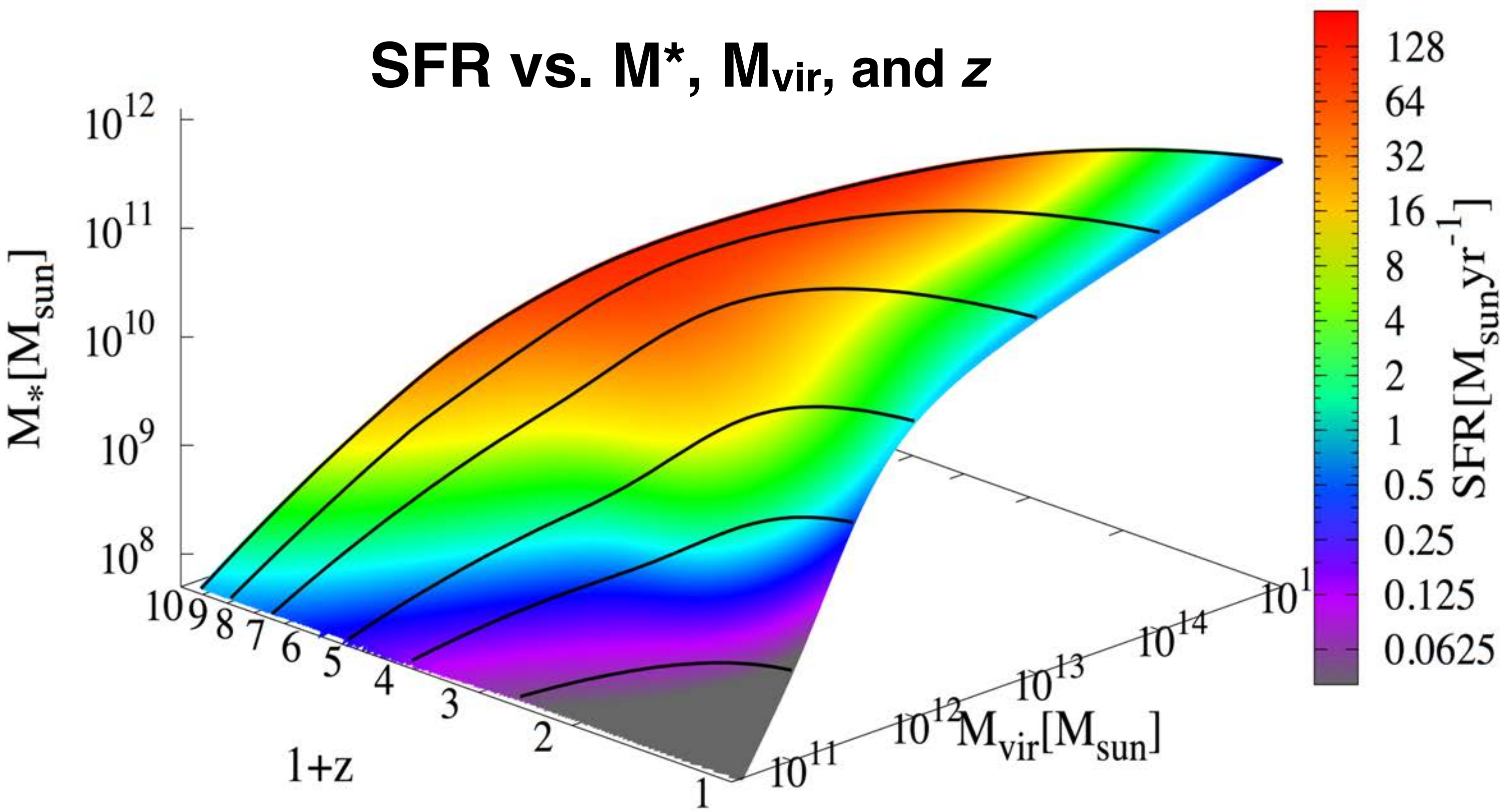

Stellar Mass-Halo Mass Relation

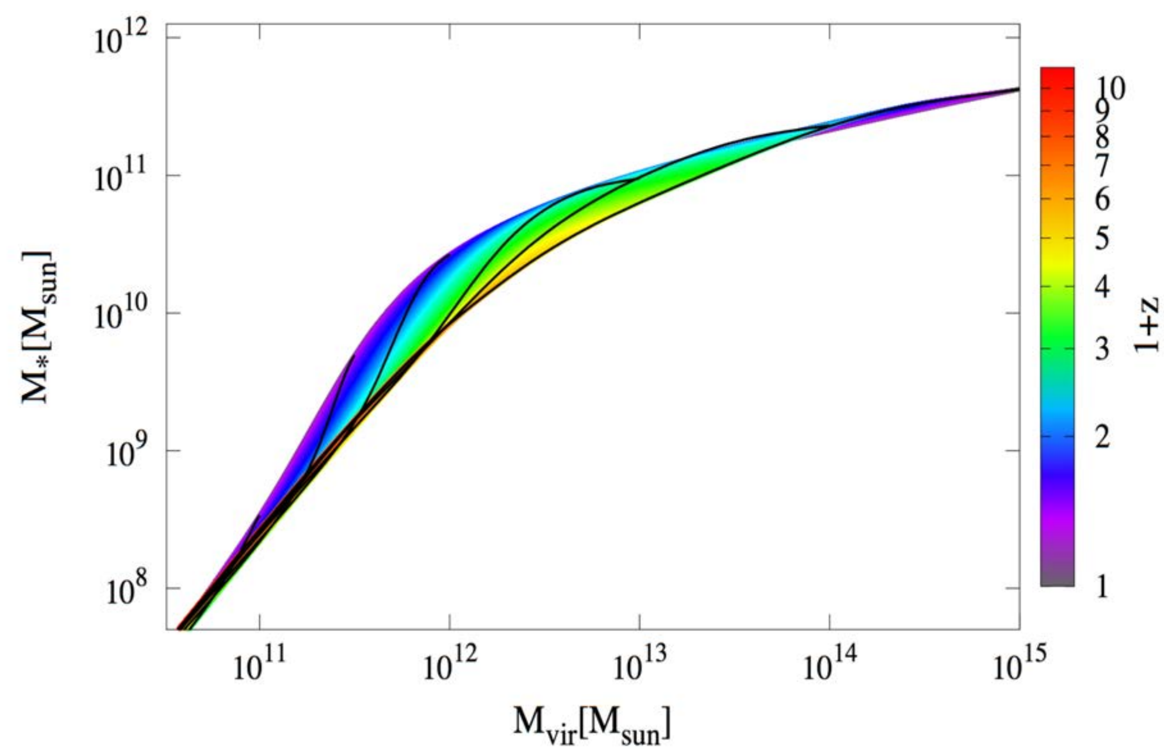

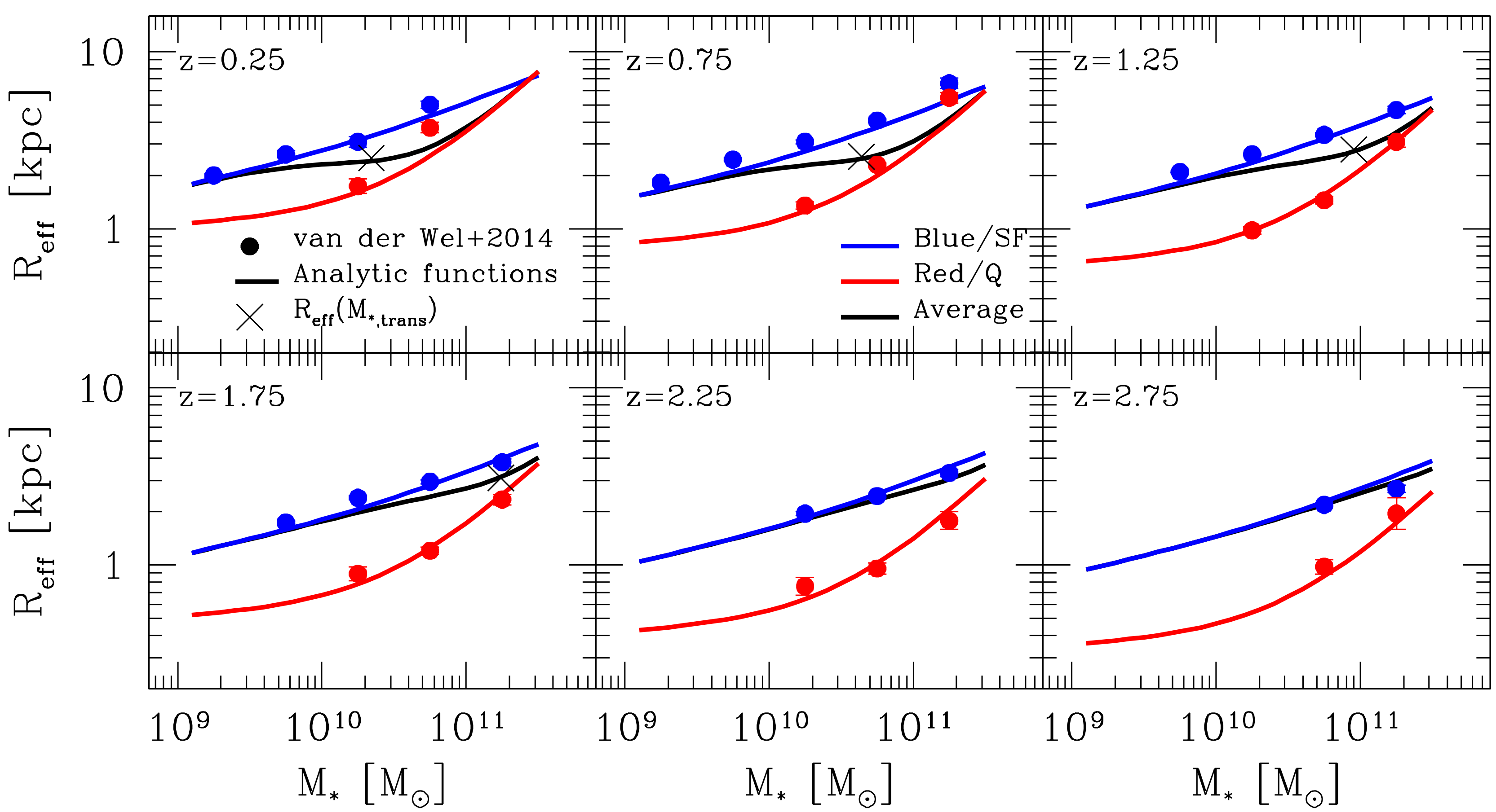

Galaxy Radial Stellar Mass Distribution

Solid lines show the redshift dependence for blue and red galaxies of the local relation by Mosleh, Williams & Franx (2013) based on the MPA-JHU SDSS DR7. The black solid lines show the average circularized effective radius as a function of stellar mass. The crosses show the effective radius at M_{50}, the stellar mass at which the quenched fraction of galaxies is 50%. We utilize the plotted redshift dependences as an input to derive the average galaxy's radial mass distribution as a function of stellar mass by assuming that blue/star-forming galaxies have a Sersic index n = 1 while red/quenched galaxies have a Sersic index n = 4.

Constraining the Galaxy Halo Connection: Star Formation Histories, Galaxy Mergers, and Structural Properties

Aldo Rodriguez-Puebla, Joel Primack, Vladimir Avila-Reese, Sandra Faber MNRAS 2017

We infer galaxy merger rates from halo mergers

Change in slope in Reff - M✷ diagram after quenching, consistent with uptick in minor merger rate and galaxy minor merger simulations

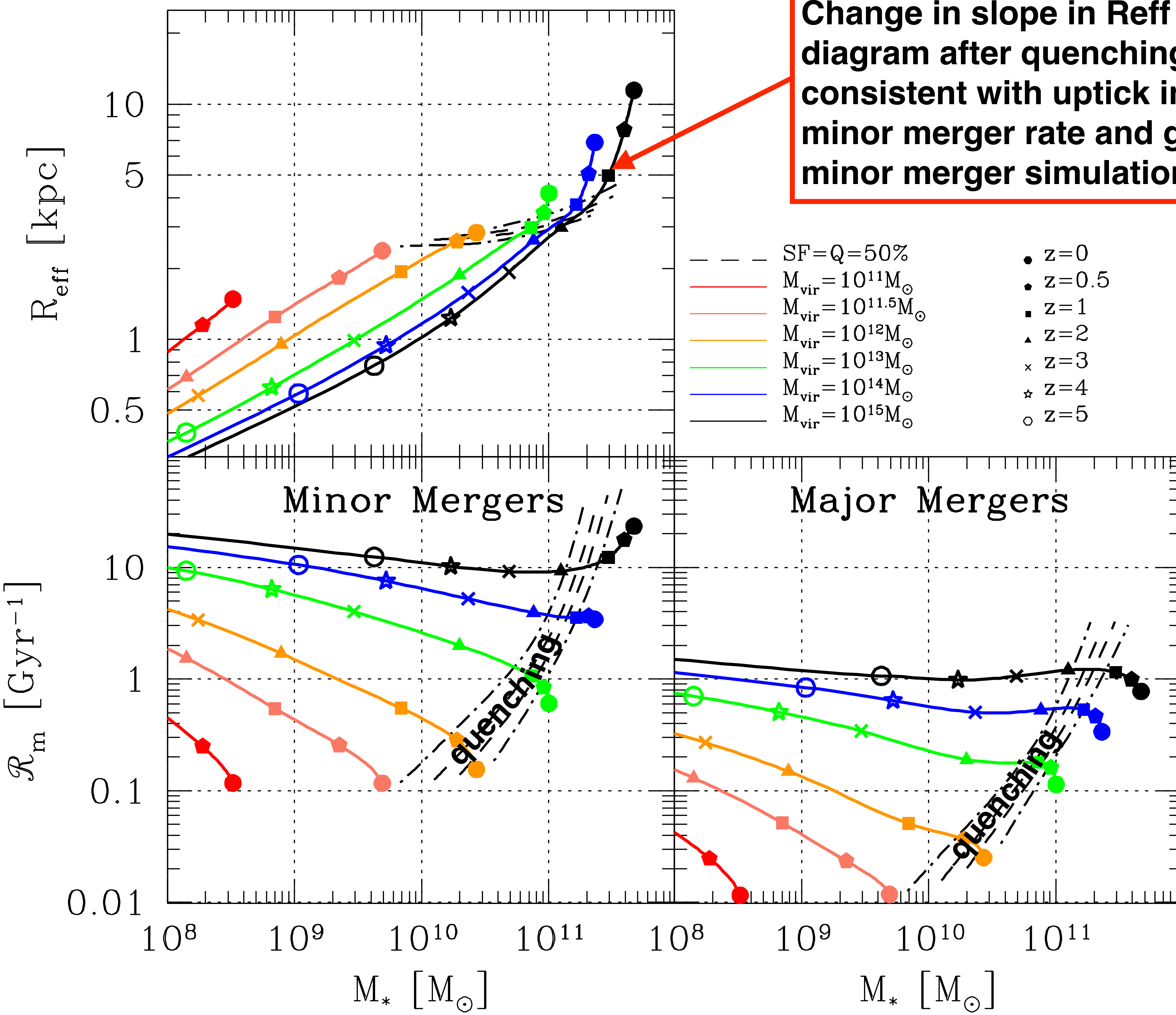

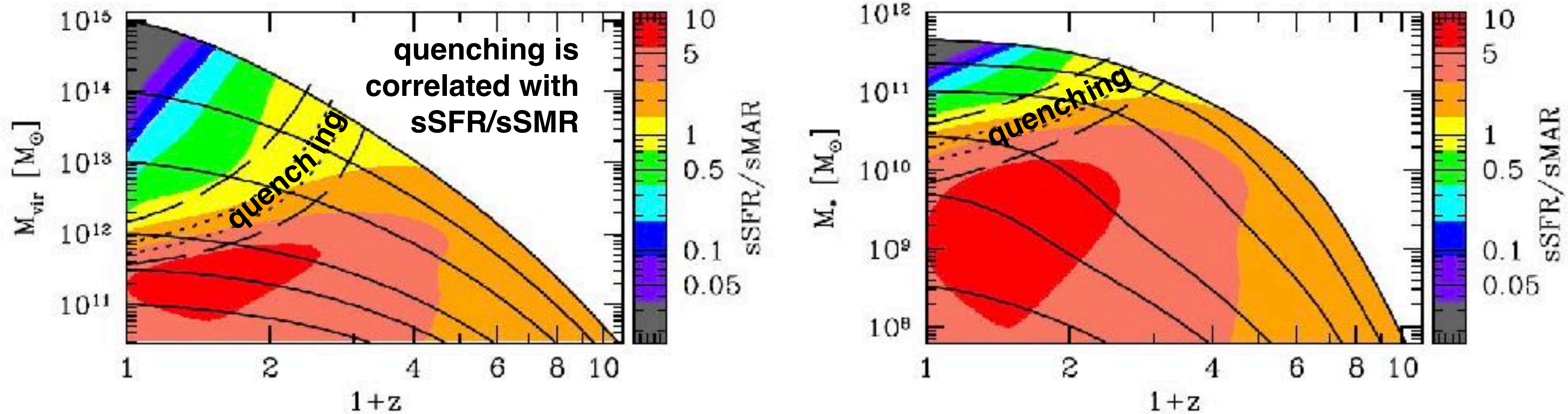

This figure shows that quenching is correlated with sSFR/sSMR = t_{halo}/t_*, since sSFR/sSMR and quenching curves are nearly parallel. sSFR/sSMR

- first rises, reaching a peak ~2 at z ~ 3 for 10^{13} halos, a peak ~7 for 10^{12} halos at z~1.5, and 10^{11} halos are still at peak sSFR/sSMR ~ 10
- then declines along all Mvir and M* progenitor tracks toward z=0.

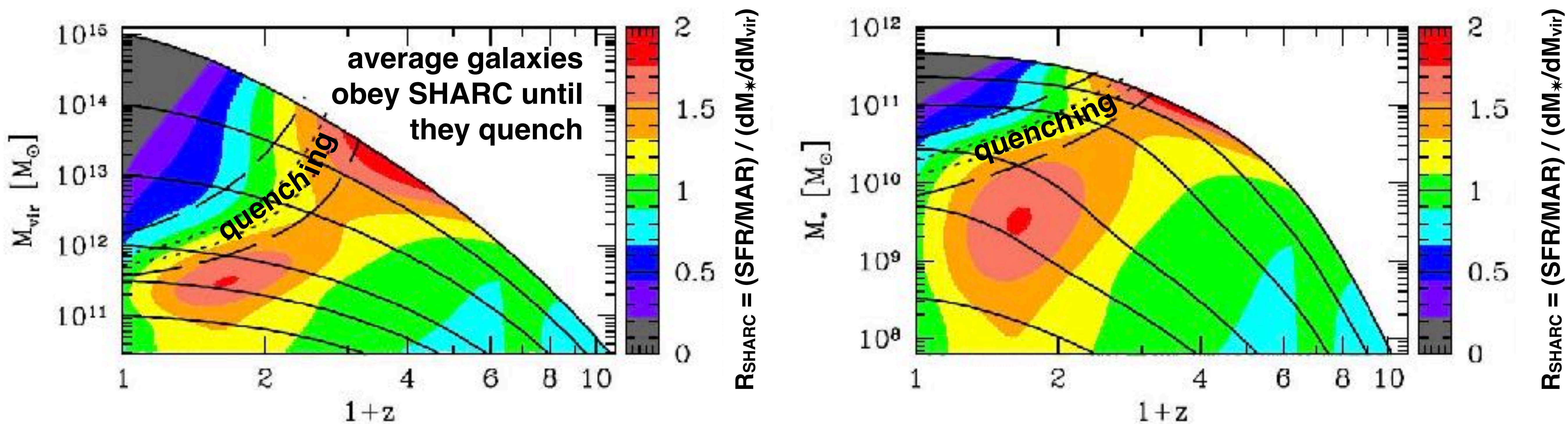

This figure shows that the SHARC approximation is rather well satisfied until quenching, the SHARC ratio R_{SHARC} = (SFR / MAR) / (dM_{vir}/dlog M*) having a value of about 1 to 2 along the progenitor trajectories, and then dropping after quenching. This shows quenching is correlated with R_{SHARC} :

- the fraction of quenched galaxies is ~ 50% when R_{SHARC} ~ 1 to 1.5, and the quenched fraction is > 75% when R_{SHARC} drops to ~1
- like sSFR/sSMR, R_{SHARC} first rises along all progenitor curves, reaches a peak at higher z for higher mass (Mvir or M*), and then declines
- unlike sSFR/sSMR, the peak SHARC ratio is nearly constant between 1.5 and 2 (the SHARC ratio peaks at about 2 for both $10^{11.5}$ halos at z ~ 0.5 and 10^{15} halos at z ~ 3, and at about 1.5 for intermediate mass halos).

Note: the SHARC formula is SFR = (dM_*/dM_{vir}) MAR where MAR = dM_{vir}/dt. Define R_{SHARC} = (SFR / MAR) / (dM_*/dM_{vir}), so SHARC ==> R_{SHARC} = 1.

Constraining the Galaxy Halo Connection: Star Formation Histories, Galaxy Mergers, and Structural Properties

Aldo Rodriguez-Puebla, Joel Primack, Vladimir Avila-Reese, Sandra Faber

MNRAS 2017

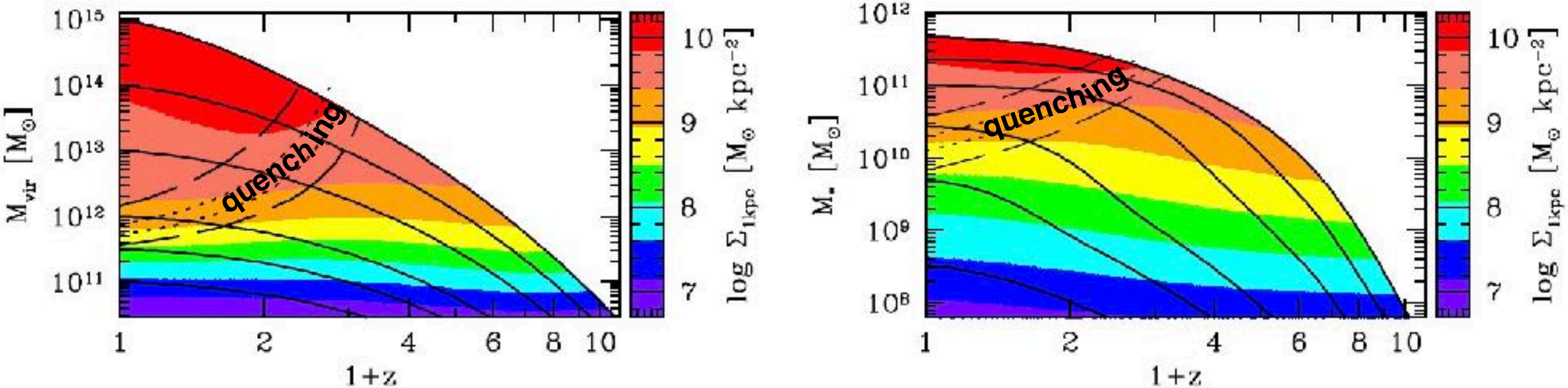

This figure (and the left panel below) shows that Σ_1 reaching a maximum correlates with quenching:

- **Σ_1 at the quenching transition rises steadily with M_{vir} and reaches maximum at lower z for lower M_{vir} — "quenching downsizing"**
- **That the progenitor tracks are parallel to the trajectory curves shows that Σ_1 remains constant after it reaches its maximum**

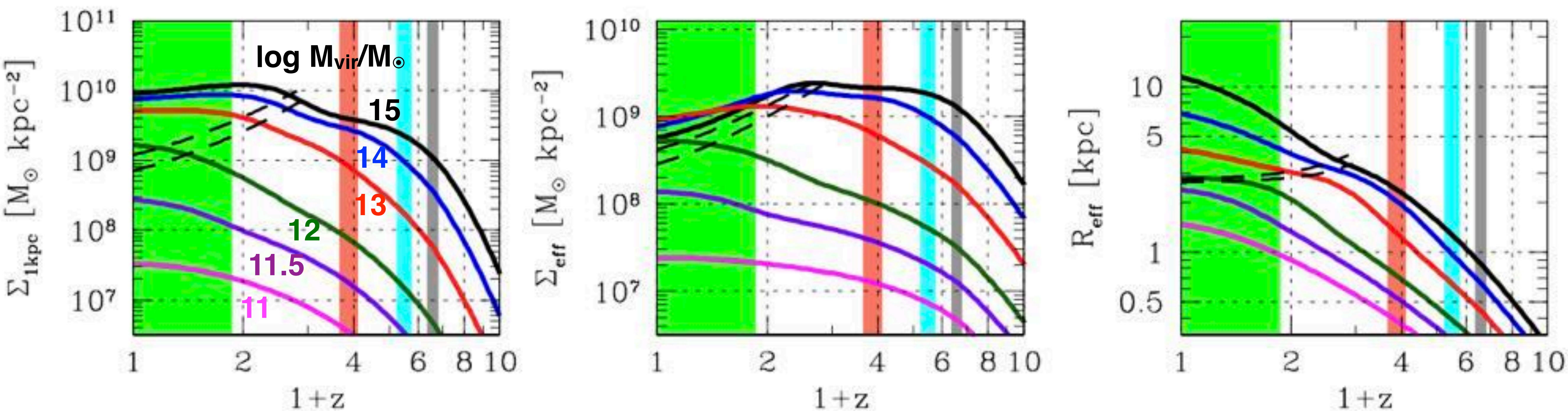

The right panel shows that R_{eff} steadily rises along halo trajectories, and quenching typically occurs when $R_{eff} \approx 3$ kpc. Although Σ_1 is flat after quenching, the middle panel shows that Σ_{eff} declines after quenching as R_{eff} increases.

https://132.248.1.39/galaxy/galaxy_halo.html

Constraining the Galaxy Halo Connection: Star Formation Histories, Galaxy Mergers, and Structural Properties

Aldo Rodriguez-Puebla, Joel Primack, Vladimir Avila-Reese, Sandra Faber (RP17) MNRAS 2017

Corresponding 2-point correlation fcns - Rodriguez-Puebla et al. in prep.

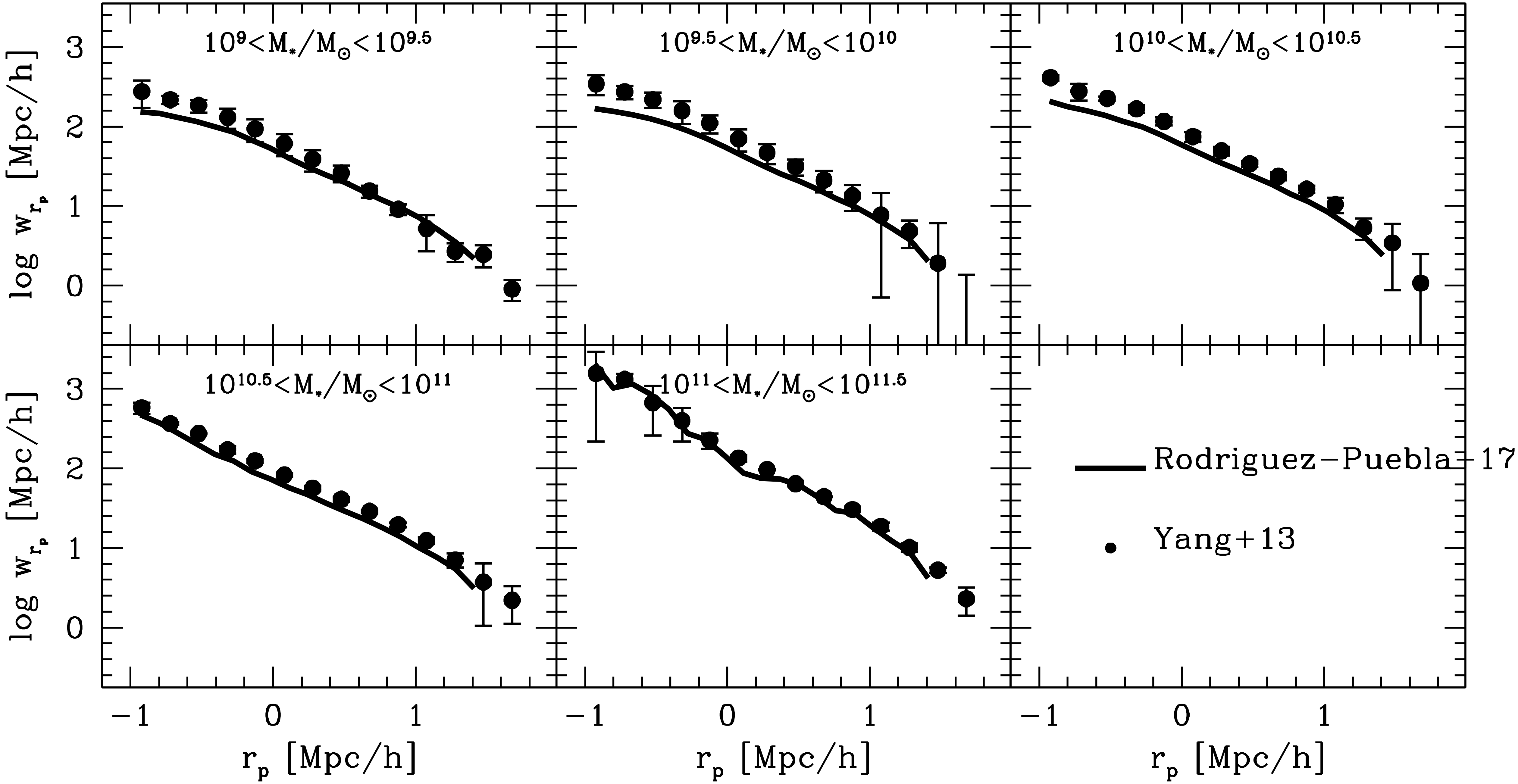

Two point correlation function in five stellar mass bins. Solid lines indicate the results of the SHAM result from RP17 while filled circles with error bars is for the SDSS analysis from Yang+12. Note that RP17 used M_{vir} for distinct halos and M_{peak} for subhalos in their SHAM analysis. The correlation function is known to be underestimated when using M_{vir} and M_{peak} rather than V_{max} and V_{peak} in SHAM (e.g., Reddick et al. 2013).

Abundance Matching LF and MF Are Independent of Density

Radu Dragomir, Aldo Rodríguez-Puebla, Joel R. Primack, Christoph T. Lee, Peter Behroozi, Doug Hellinger, Avishai Dekel (in preparation)

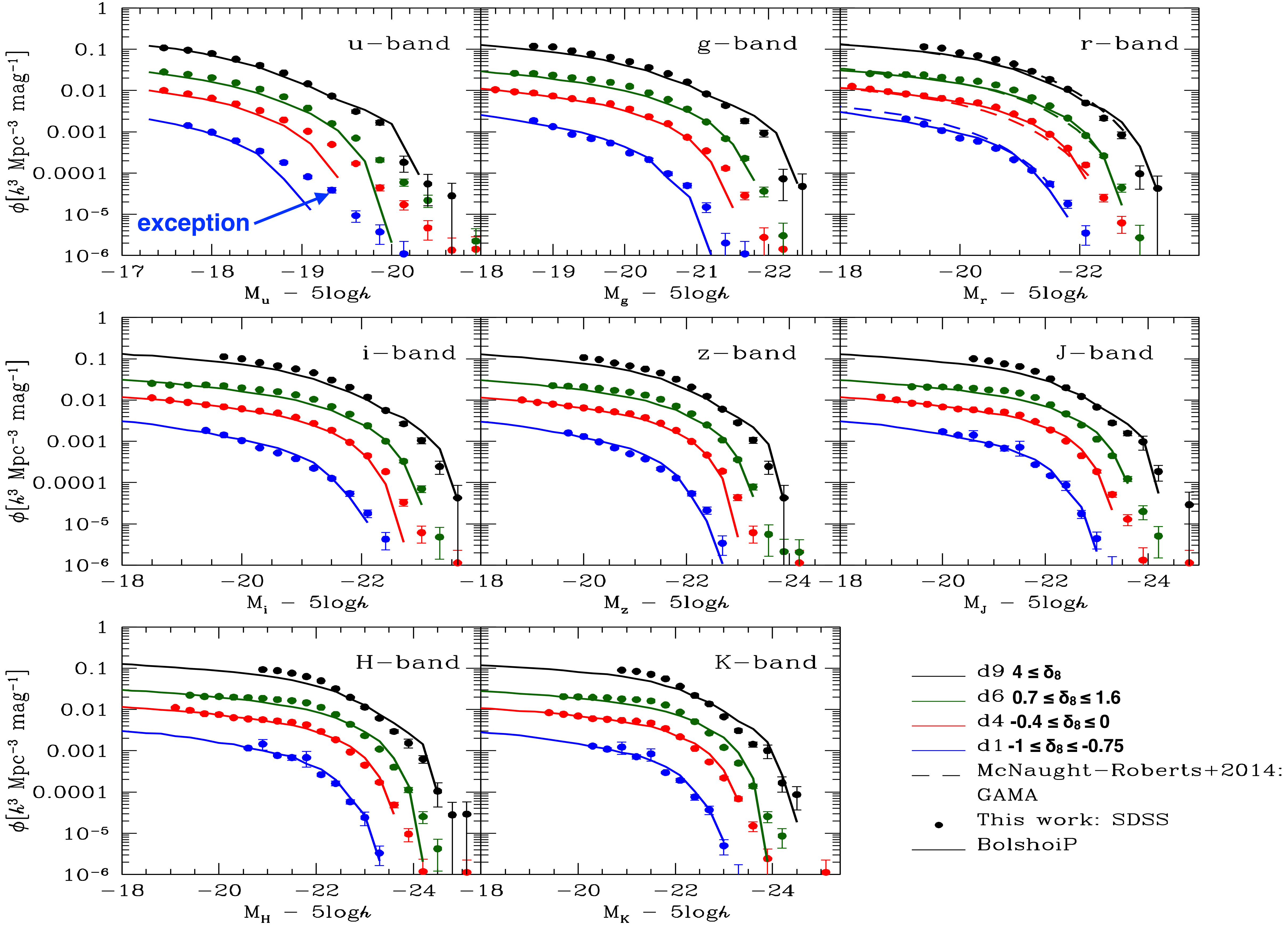

Abundance Matching LF and MF Are Independent of Density

Radu Dragomir, Aldo Rodríguez-Puebla, Joel R. Primack, Christoph T. Lee,
Peter Behroozi, Doug Hellinger, Avishai Dekel (in preparation)

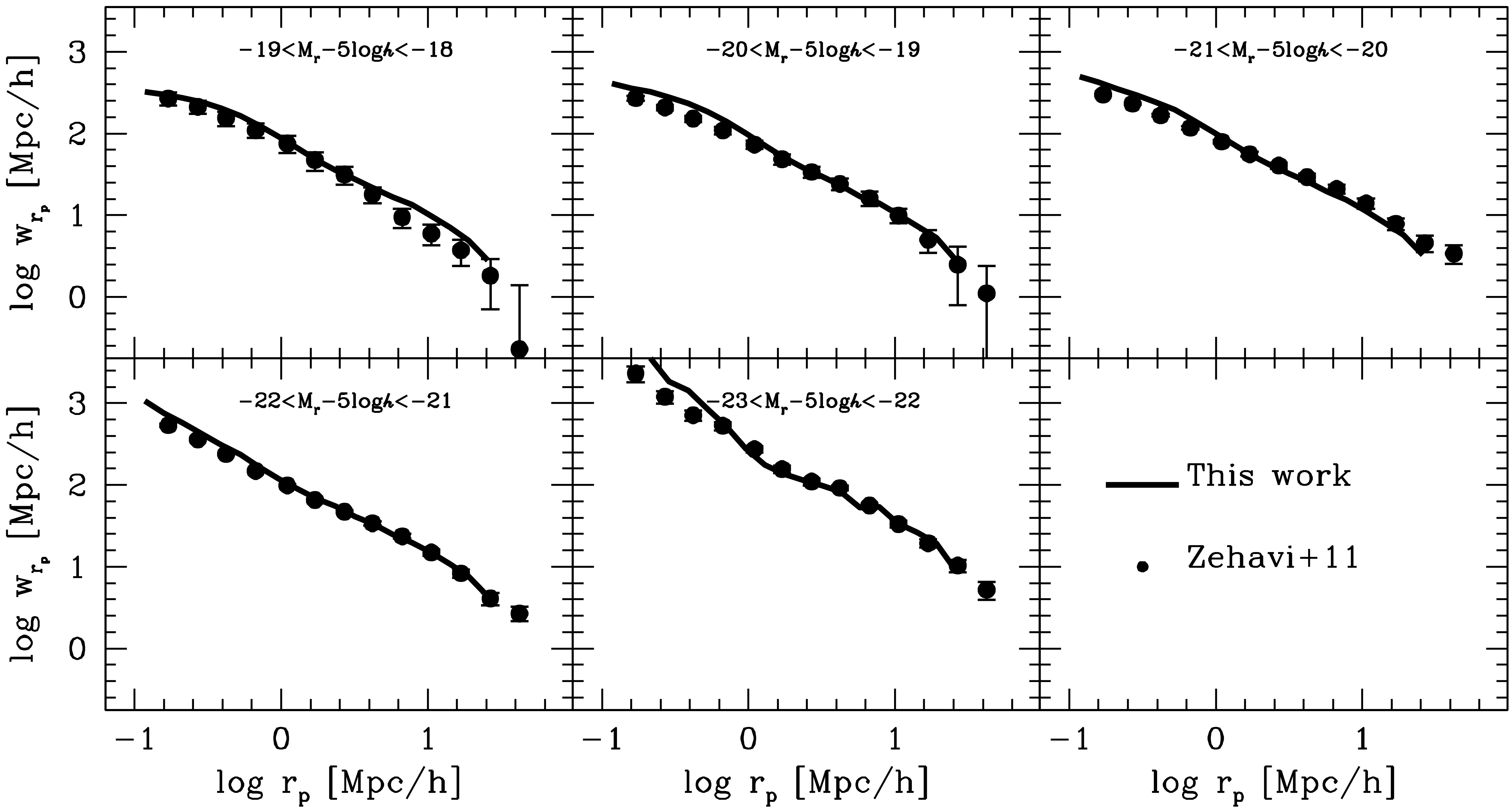

Two point correlation function in five r-band luminosity bins. Solid lines indicate the results of the SHAM result from Radu Dragomir et al. in prep., while filled circles with error bars are for the SDSS analysis from Zehavi+2011. Dragomir et al. in prep. uses V_{max} for distinct halos and V_{peak} for subhalos.

Abundance Matching LF and MF Are Independent of Density

Radu Dragomir, Aldo Rodríguez-Puebla, Joel R. Primack, Christoph T. Lee, Peter Behroozi, Doug Hellinger, Avishai Dekel

(in preparation)

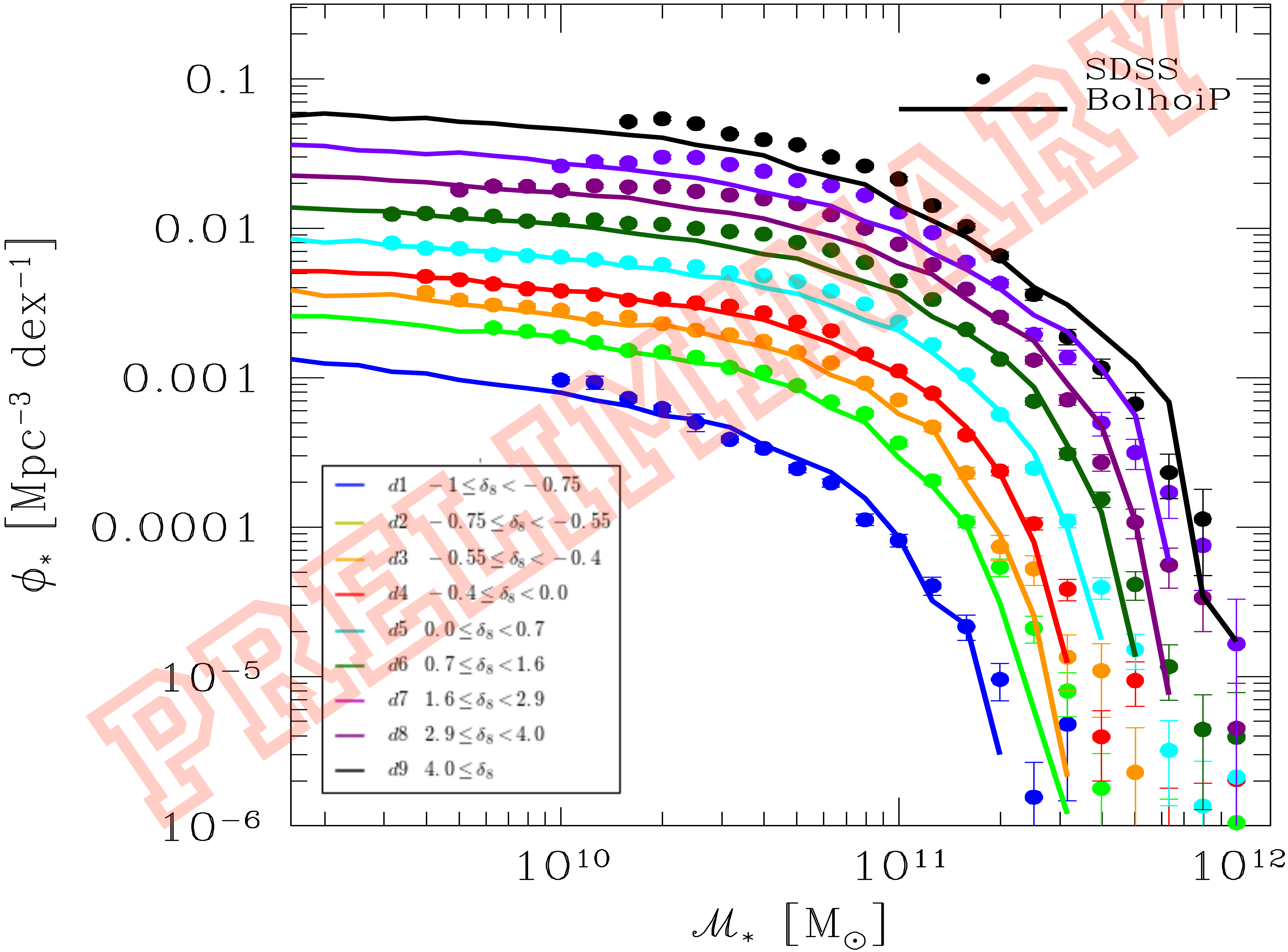

Abundance Matching LF and MF Are Independent of Density

Radu Dragomir, Aldo Rodríguez-Puebla, Joel R. Primack, Christoph T. Lee, Peter Behroozi, Doug Hellinger, Avishai Dekel (in preparation)

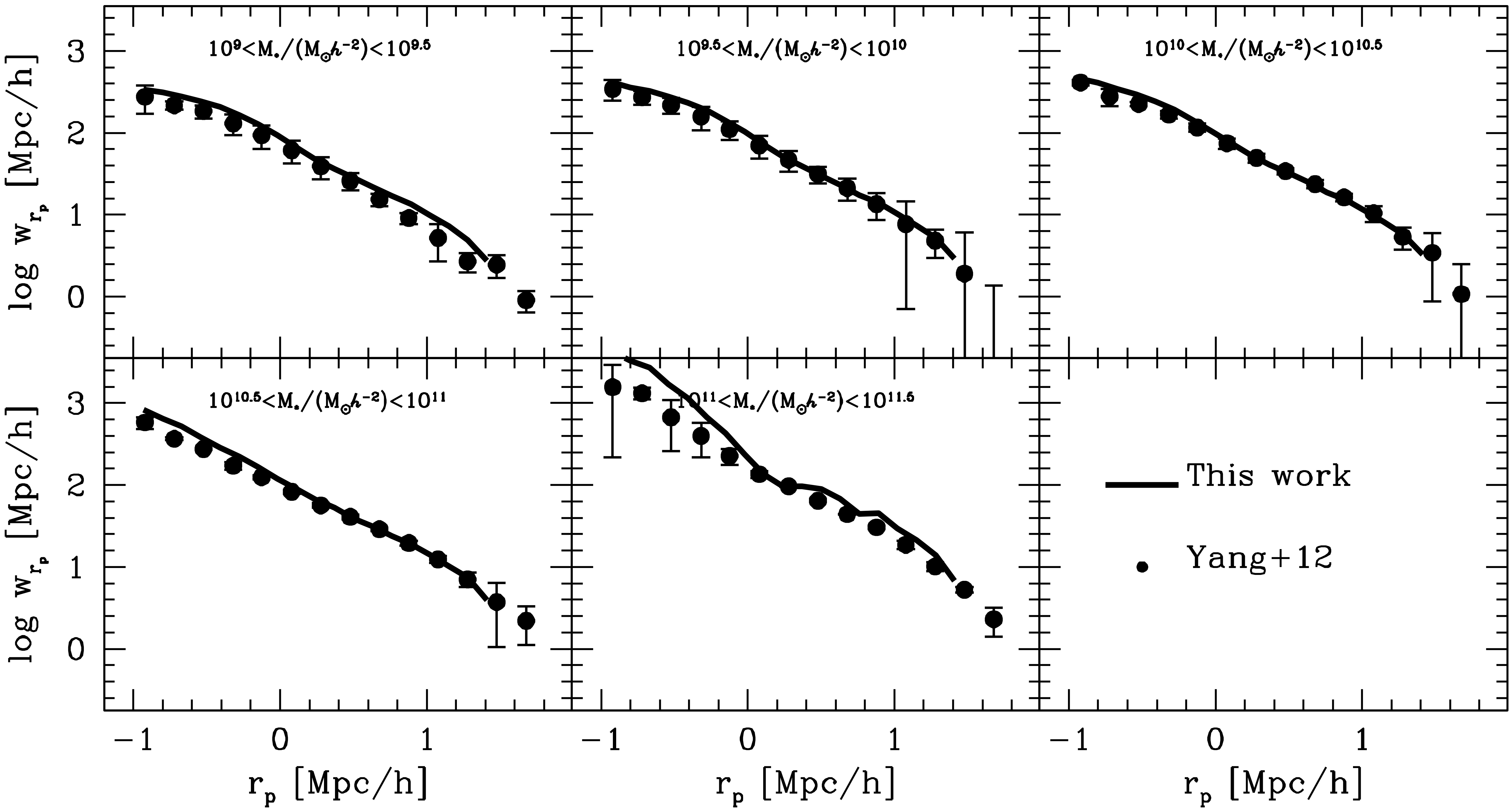

Two point correlation function in five stellar mass bins. Solid lines indicate the results of the SHAM result from Radu in prep. while filled circles with error bars is for the SDSS analysis from Yang+12. In this case Dragomir et al. in prep. uses V_{max} for distinct halos and V_{peak} for subhalos in the SHAM analysis. Note that this SHAM reproduces the two point correlation function and the stellar mass function in various environments at the same time.

Causes & Consequences of Halo Mass Loss

Christoph T. Lee, Joel R. Primack, Peter Behroozi, Aldo Rodríguez-Puebla, Doug Hellinger, Austin Tuan, Jessica Zhu, Avishai Dekel **in final prep.**

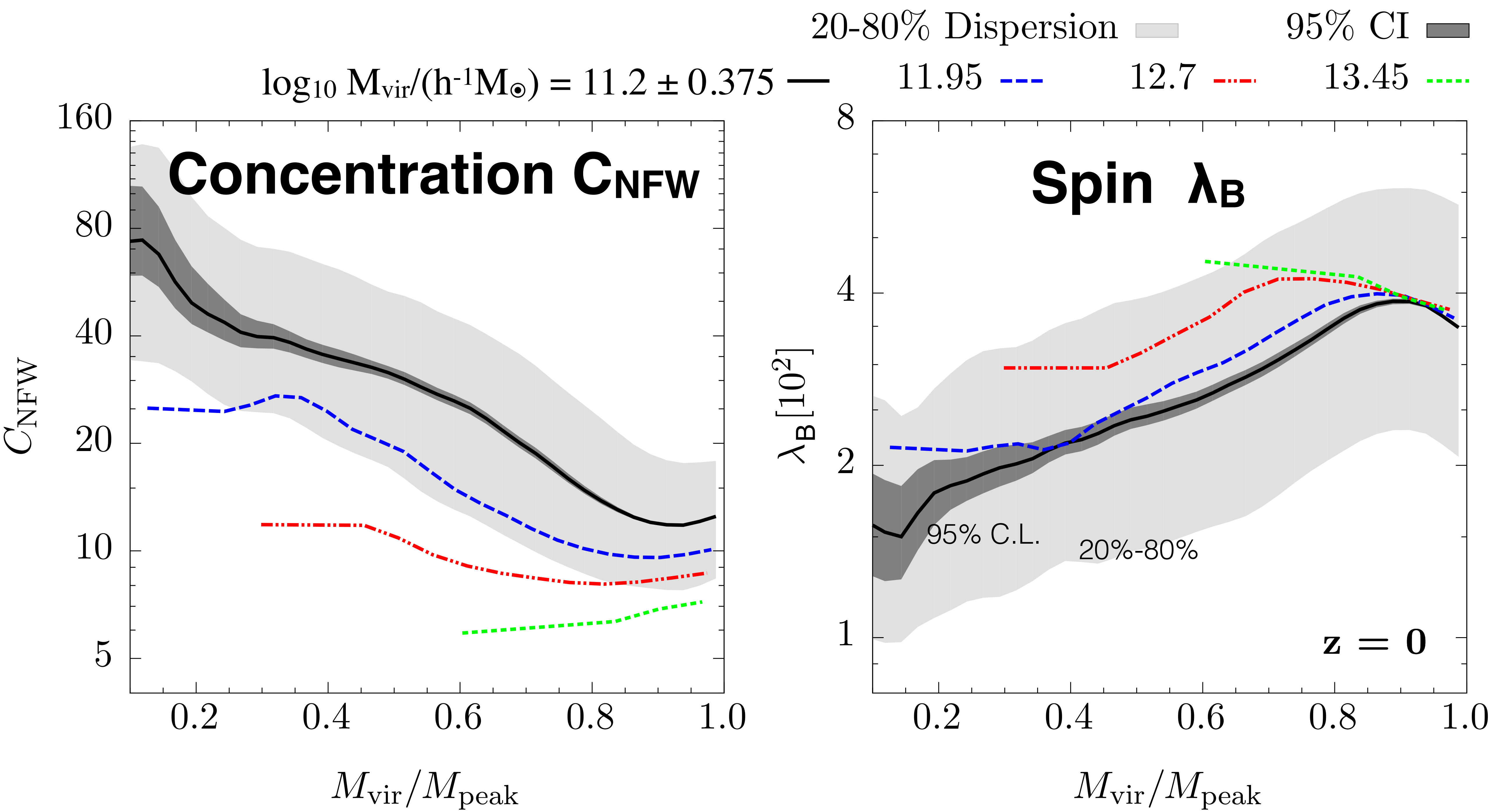

- **Most low mass halos in dense regions are significantly stripped**
- **Halos that have lost 5-15% of their mass relative to M_{peak} have lower C_{NFW}, higher λ_B**
- **Halos that have lost more than ~20% of their mass have higher C_{NFW} and lower λ_B**

Causes & Consequences of Halo Mass Loss

Christoph Lee

GalHalo17-Conference Poster

Tidal Stripping:

Strong tidal force from a nearby massive halo removes loosely bound particles from a halo. 40% of tidally stripped low mass halos lose more than 20% of their peak mass. Tidally stripped halos develop:

- **Low NFW scale radius** (high concentration) due to steepening outer profile
- **Low spin parameter** due to preferential removal of high angular momentum material
- **Low prolateness** (they become rounder) due to preferential removal of particles on highly elliptical orbits.

Evaporation:

Major mergers typically cause **temporary jumps in NFW scale radius, spin parameter, and shape**. As halos relax after a merger, they shed high energy material (evaporate) and **settle back to lower values of scale radius, spin parameter, shape, and viral ratio**. After a major merger, halos typically lose 5-15% of their peak mass through evaporation.

Examples of individual halo evolution

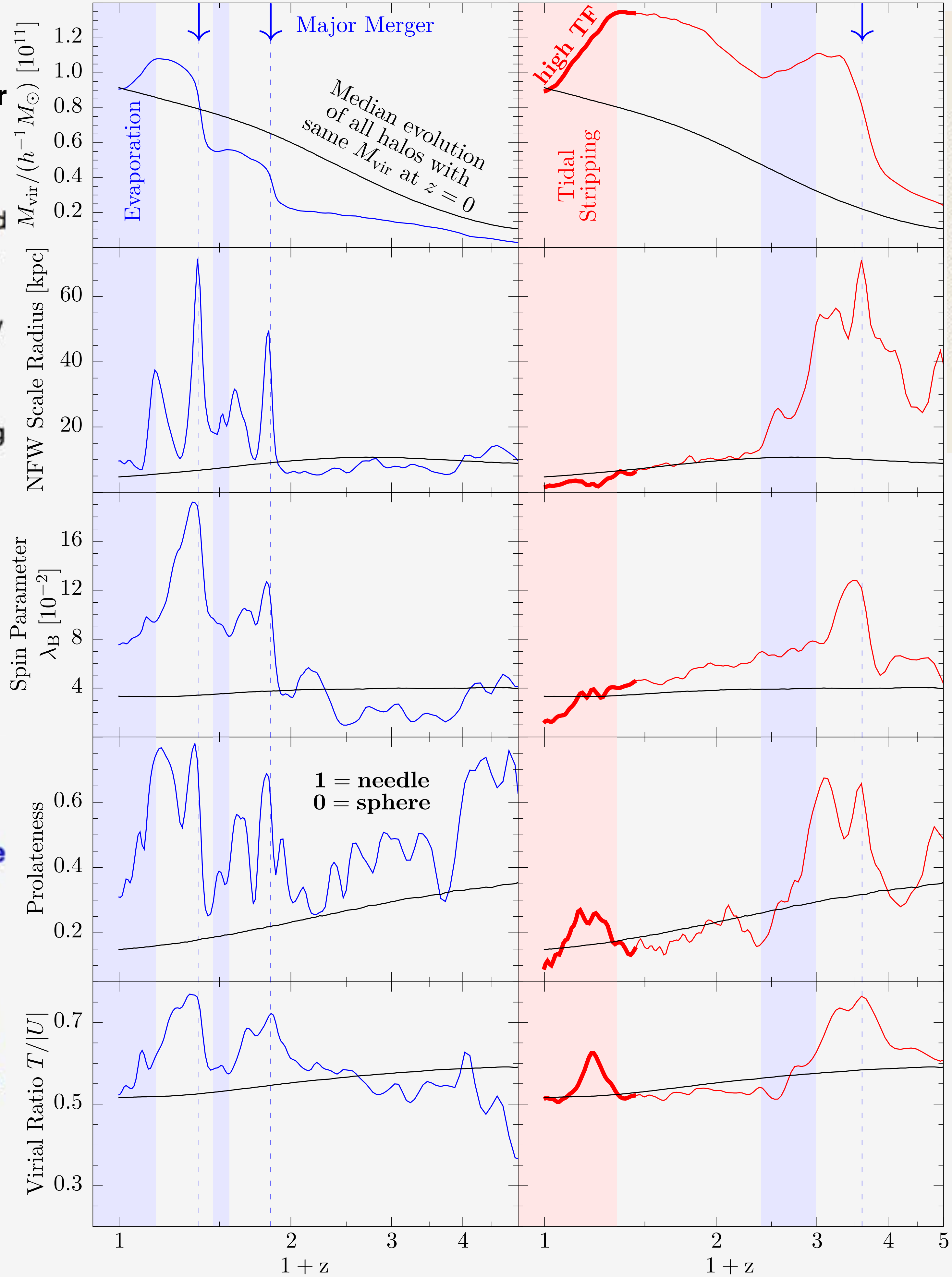

Is halo mass loss common?

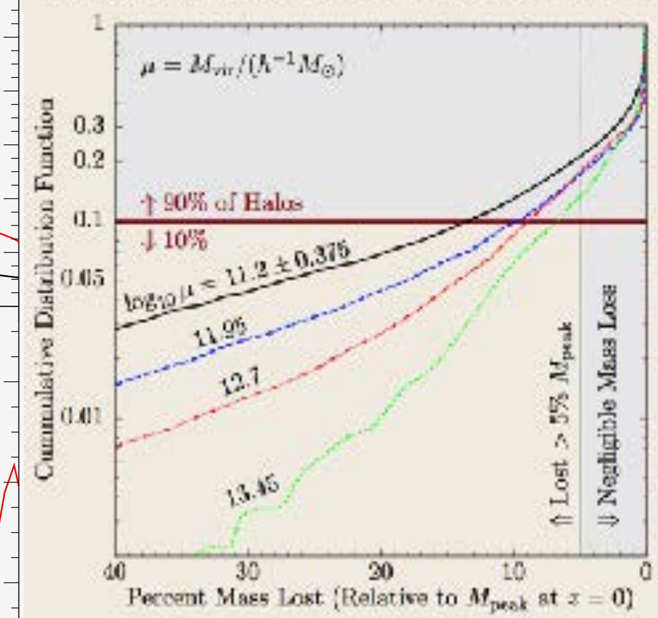

Extending this analysis to all halos

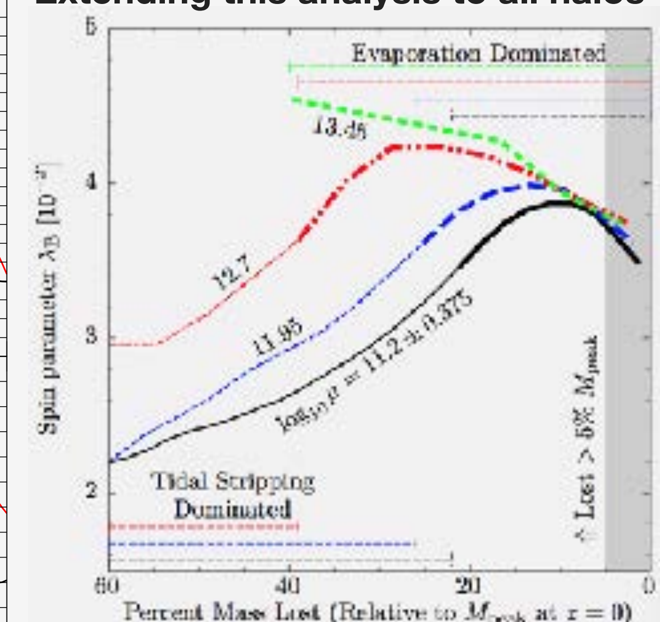

- Low mass halos (log μ =11.2) that have lost 5-15% of their peak mass most commonly experienced evaporative mass loss (temporarily high spin parameters).
- Low mass halos that have lost greater than 20% of their peak mass typically are actively being tidally stripped (low spin parameters). More heavily stripped halos have lower spin parameters.
- Some low mass halos are strongly affected by tidal stripping, while high mass halos predominantly experience evaporative mass loss.

Causes & Consequences of Halo Mass Loss

Christoph T. Lee, Joel R. Primack, Peter Behroozi, Aldo Rodríguez-Puebla, Doug Hellinger, Austin Tuan, Jessica Zhu, Avishai Dekel **in final prep.**

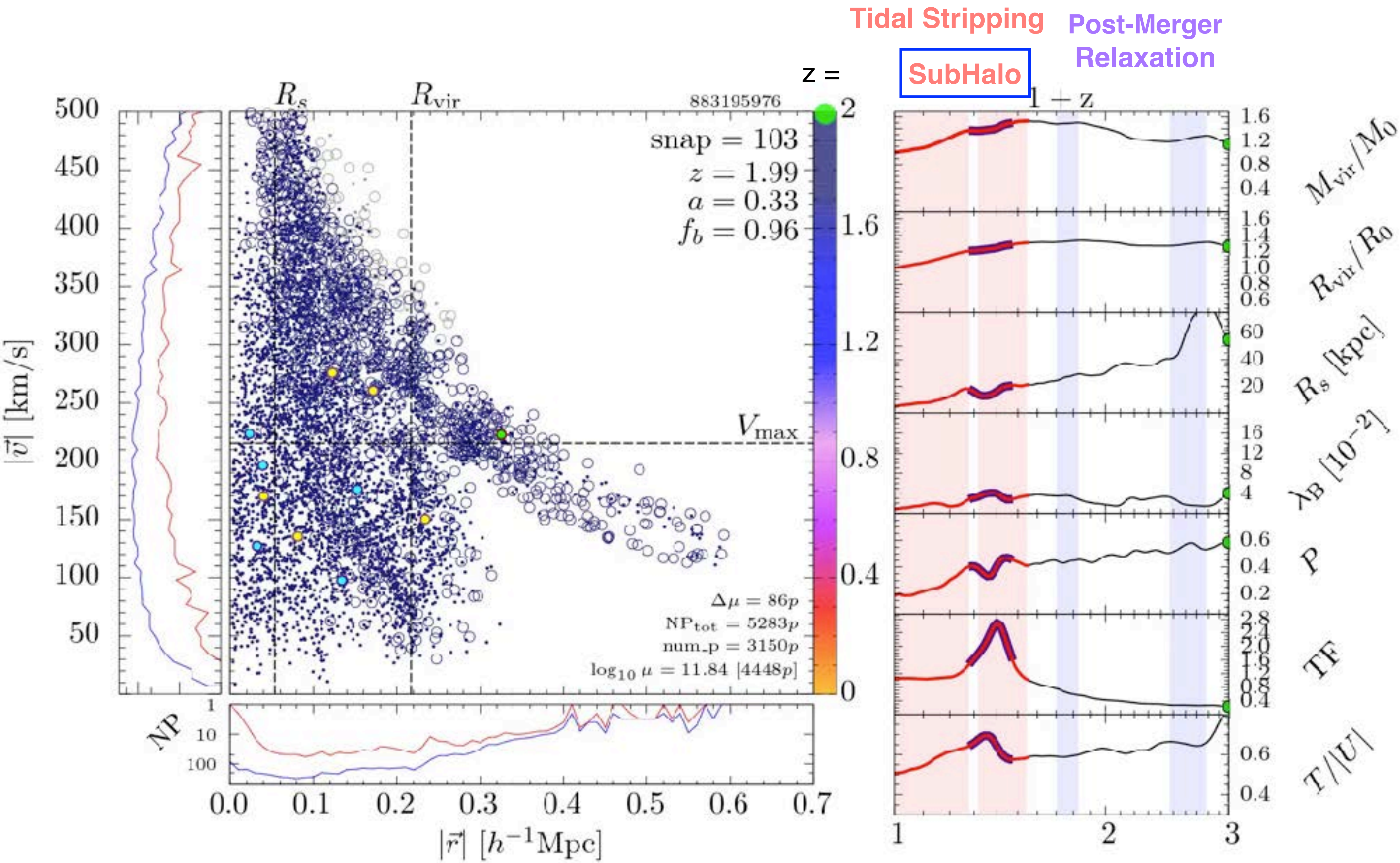

Properties of Dark Matter Haloes: Local Environment Density

Christoph T. Lee, Joel R. Primack, Peter Behroozi, Aldo Rodríguez-Puebla, Doug Hellinger, Avishai Dekel MNRAS 2017

Low Mass | **Intermediate Mass** | **High Mass**

$\log_{10} M_{vir}/(h^{-1}M_\odot) = 11.200\pm0.375$ | 11.95 ± 0.375 | 12.70 ± 0.375 | 13.45 ± 0.375

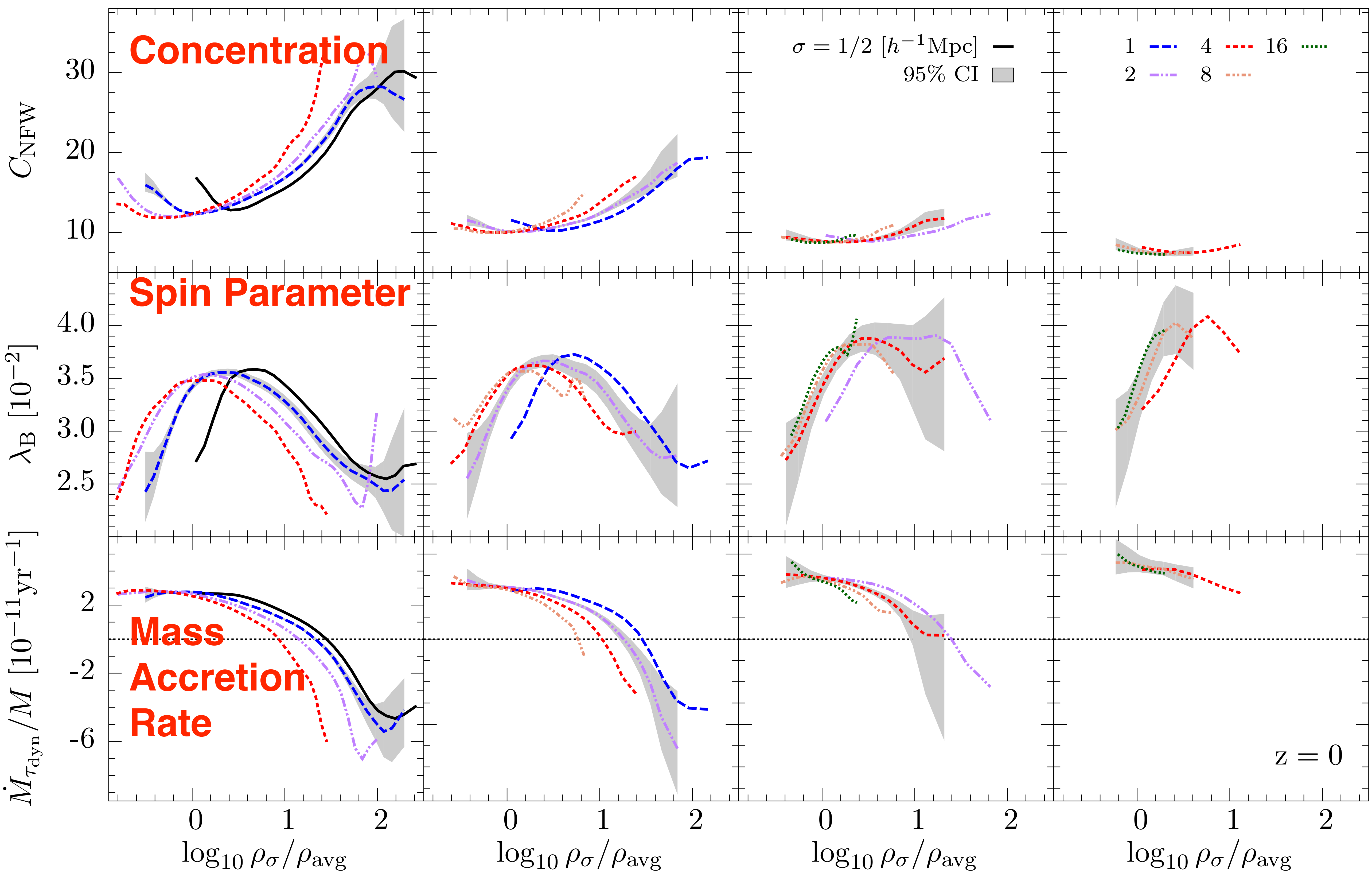

Halo Properties Independent of Web Location at the Same Density

Tze Ping Goh, Christoph T. Lee, Joel R. Primack, Miguel Aragon Calvo, Peter Behroozi, Aldo Rodríguez-Puebla, Doug Hellinger, Avishai Dekel, Kathryn Johnston (in preparation)

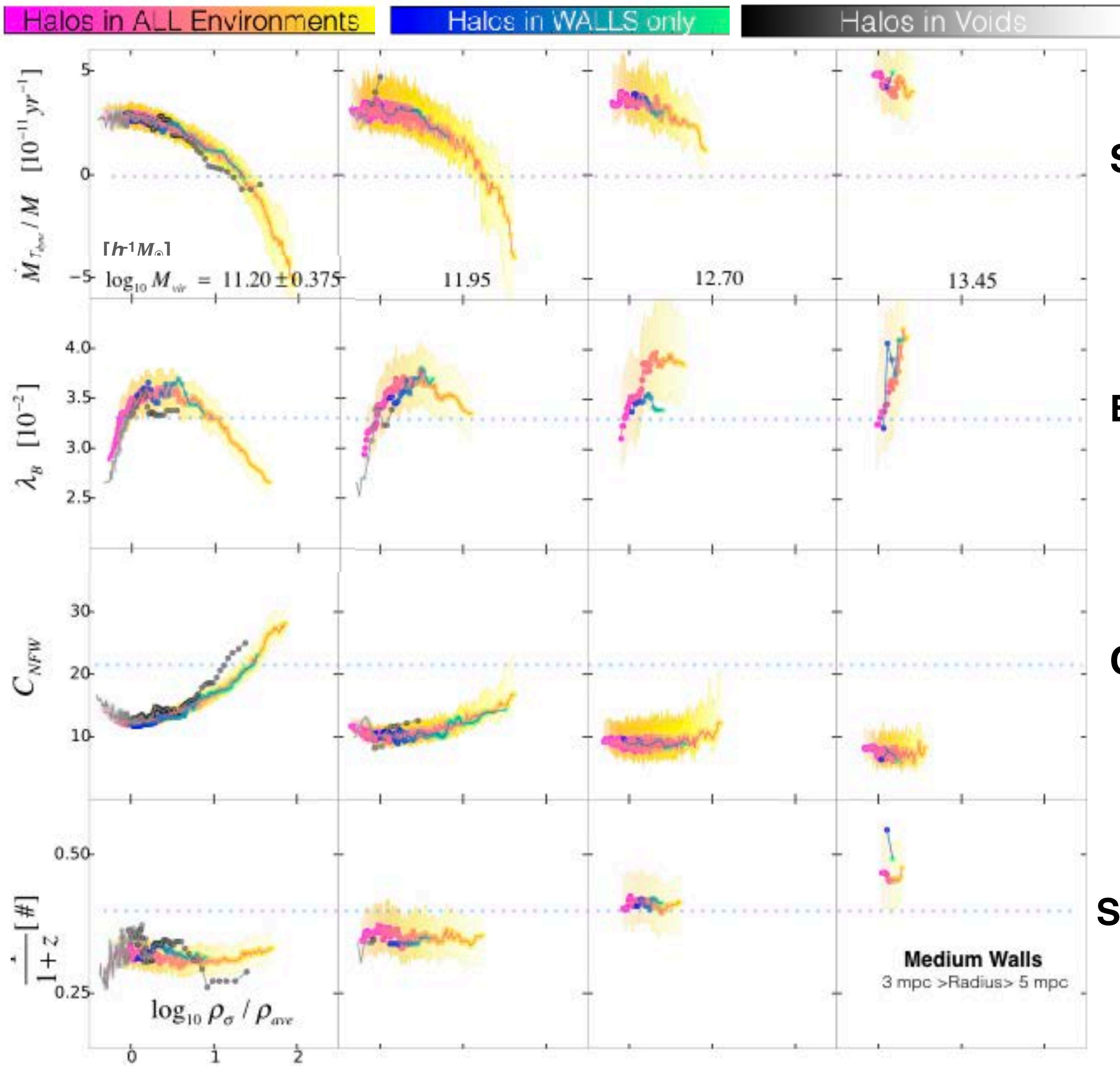

Specific Mass Accretion Rate

Bullock+2001 Spin Parameter λ_B

Concentration $C_{NFW} = R_{vir}/R_s$

Scale Factor of Last Major Merger

Halo Properties Independent of Web Location at the Same Density

Tze Ping Goh, Christoph T. Lee, Joel R. Primack, Miguel Aragon Calvo, Peter Behroozi, Aldo Rodríguez-Puebla, Doug Hellinger, Avishai Dekel, Kathryn Johnston (in preparation)

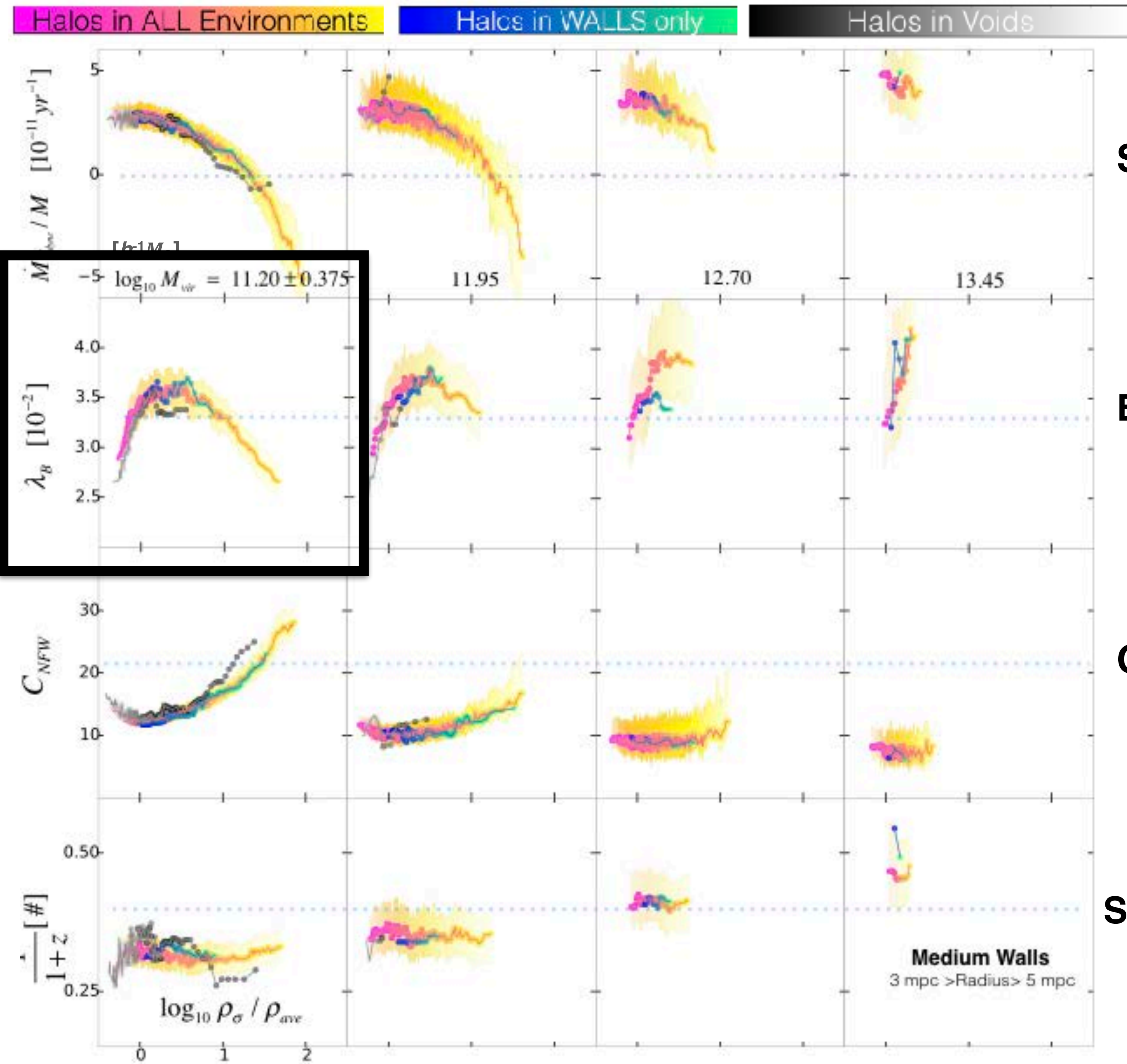

Specific Mass Accretion Rate

Bullock+2001 Spin Parameter λ_B

Concentration $C_{NFW} = R_{vir}/R_s$

Scale Factor of Last Major Merger

Halo Properties Independent of Web Location at the Same Density

Tze Ping Goh, Christoph T. Lee, Joel R. Primack, Miguel Aragon Calvo, Peter Behroozi, Aldo Rodríguez-Puebla, Doug Hellinger, Avishai Dekel, Kathryn Johnston (in preparation)

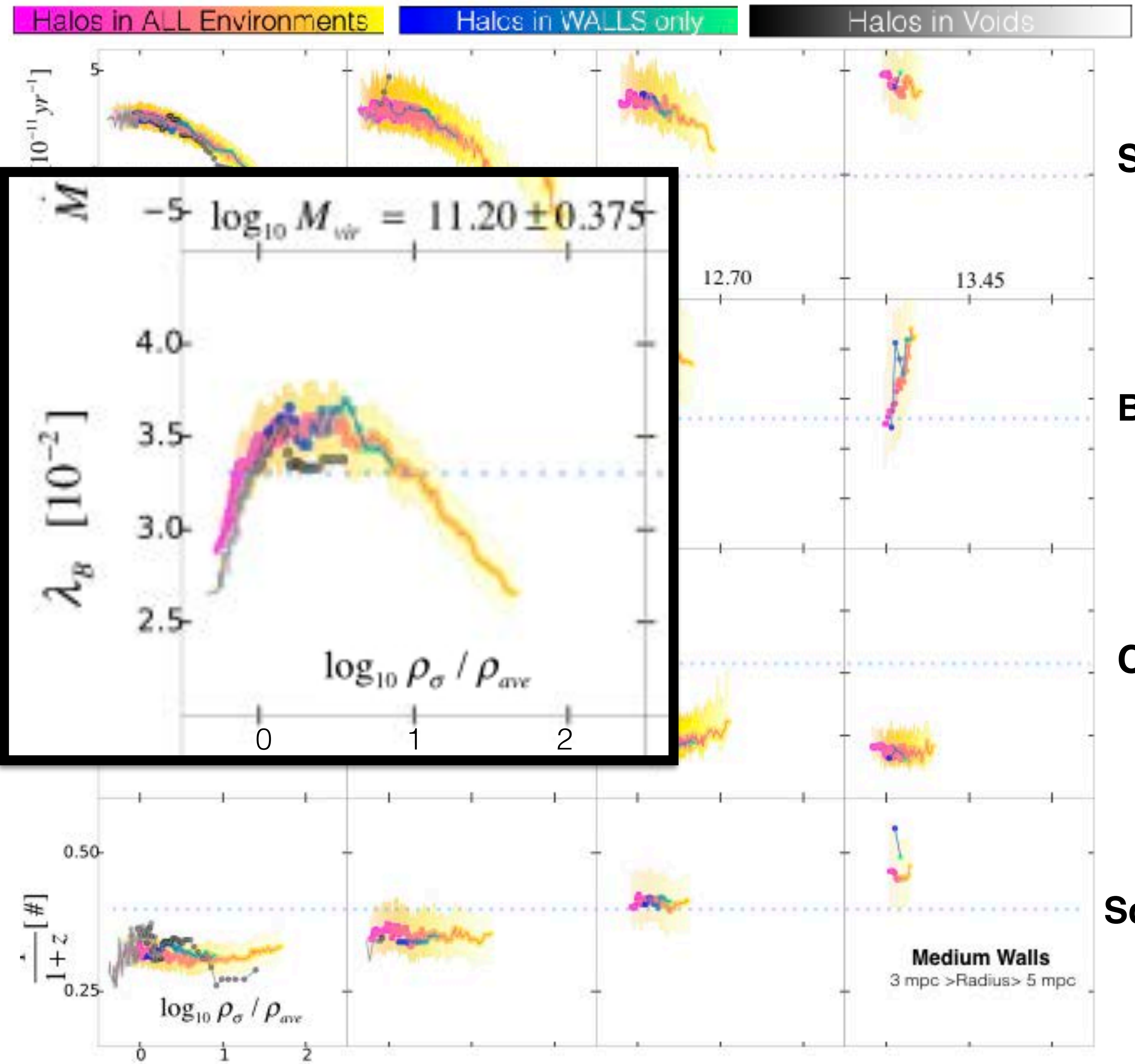

Specific Mass Accretion Rate

Bullock+2001 Spin Parameter λ_B

Concentration $C_{NFW} = R_{vir}/R_s$

Scale Factor of Last Major Merger

Halo Properties Independent of Web Location at the Same Density

Tze Ping Goh, Christoph T. Lee, Joel R. Primack, Miguel Aragon Calvo, Peter Behroozi, Aldo Rodríguez-Puebla, Doug Hellinger, Avishai Dekel, Kathryn Johnston (in preparation)

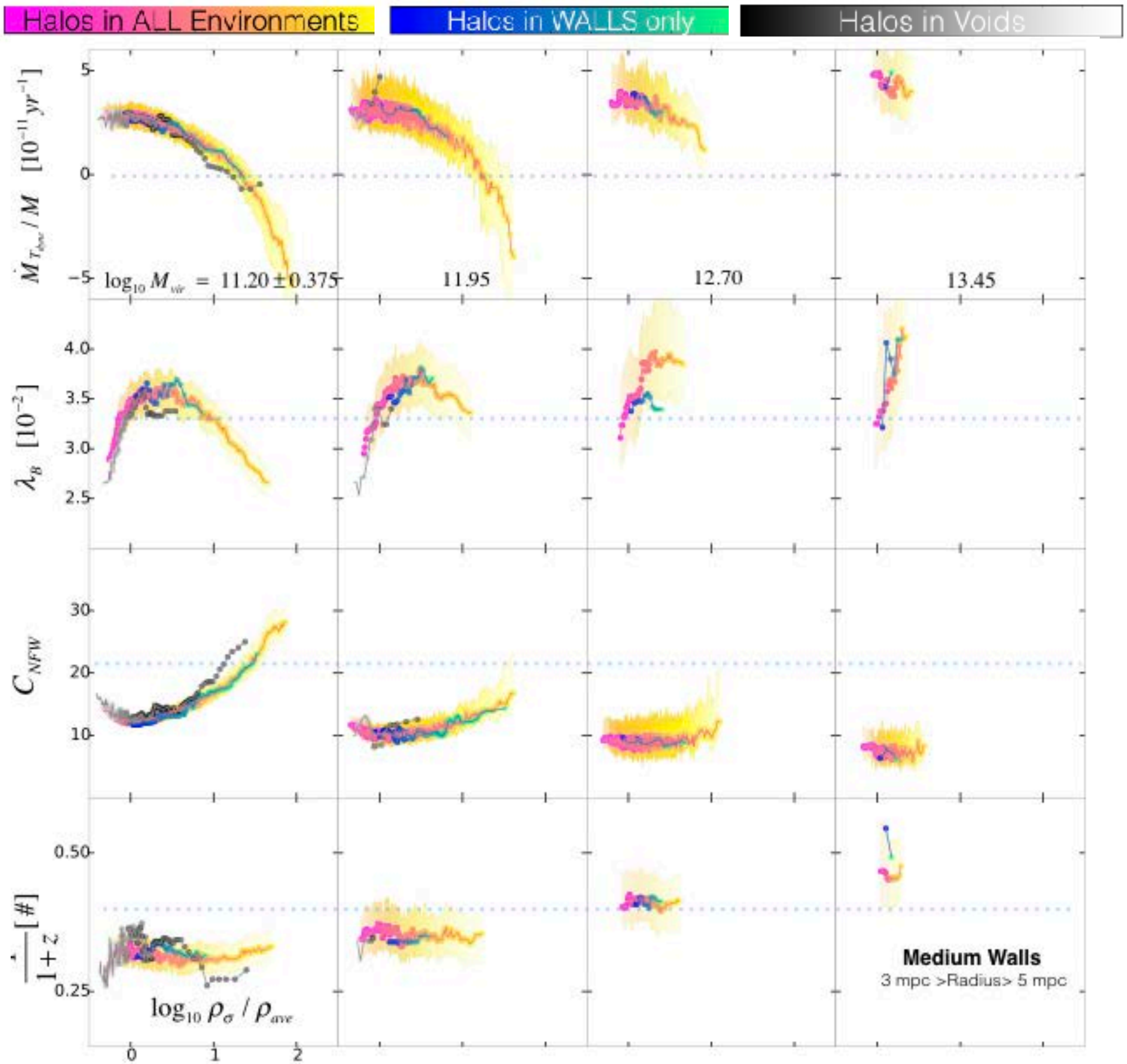

At the same environmental density, halo properties are independent of cosmic web location. It doesn't matter whether a halo is in a cosmic void, wall, or filament, what matters is the halos's environmental density. The properties studied are mass accretion rate, spin, halo concentration, scale factor of the last major merger, and prolateness. We had expected that a web's cosmic web location would matter for at least some of these halo properties. That it does not is a significant discovery.

SDSS galaxy mass and size are independent of web environment at fixed density (Yan, Fan, White 2013). GAMA data show that the galaxy luminosity function is also independent of web environment at fixed density (Eardley et al. MNRAS 2015). This contrasts with the finding that the halo mass function is dependent on web location at the same density using the v-web (Metuki, Liebeskind, Hoffman 2016).

Prolate Galaxies Dominate at High Redshifts & Low Masses

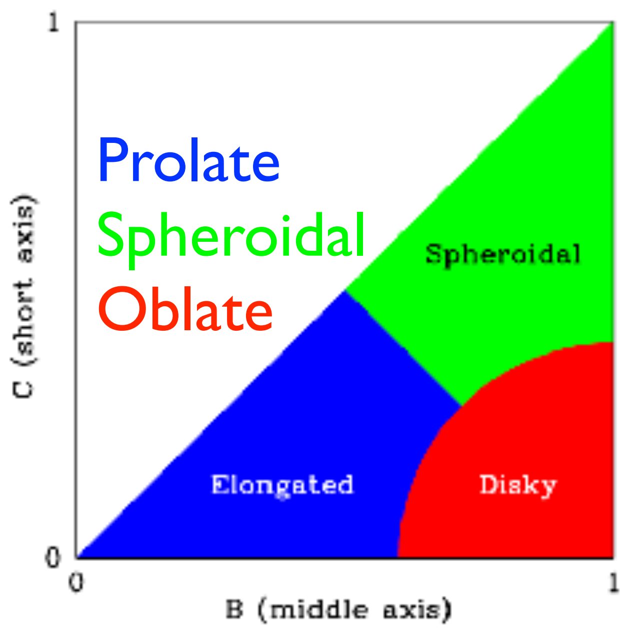

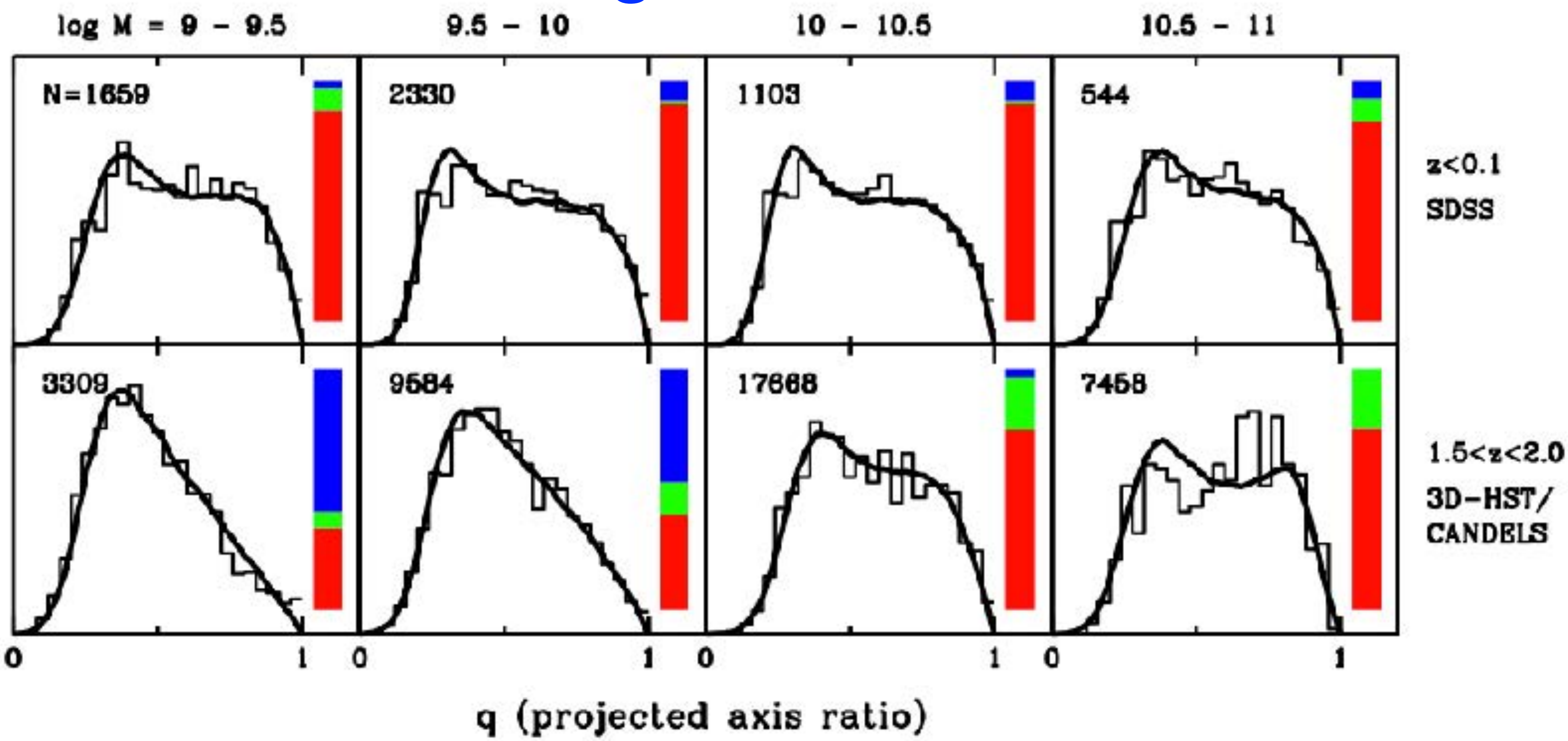

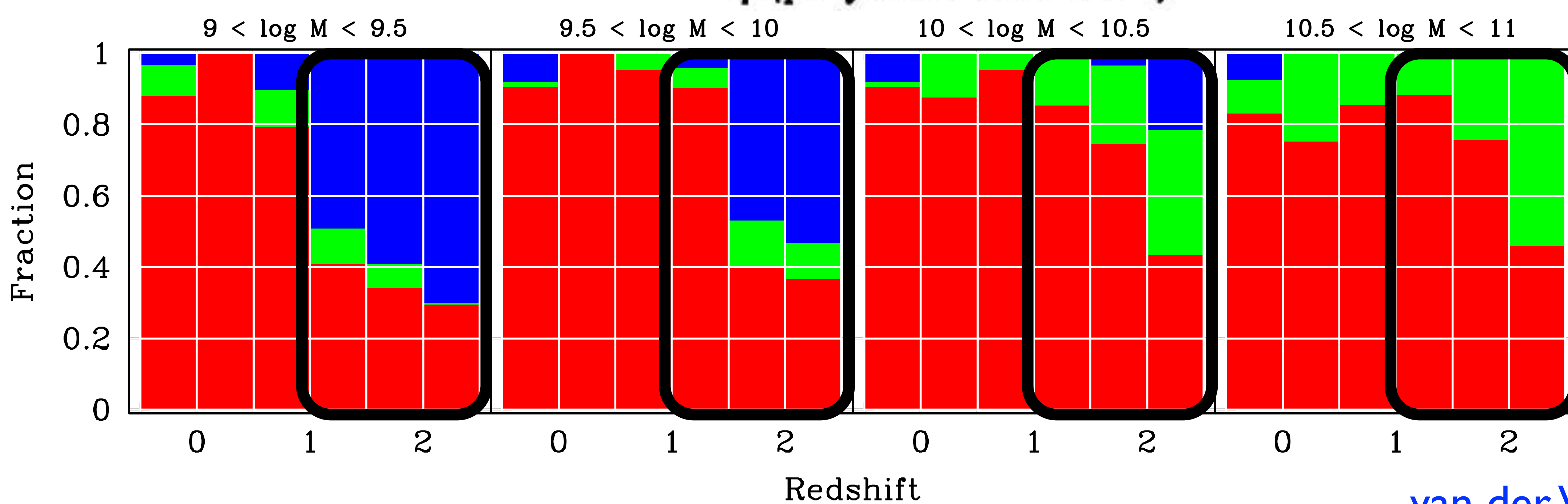

van der Wel+2014

See also Morphological Survey of Galaxies z=1.5-3.6 Law, Steidel+ ApJ 2012

When Did Round Disk Galaxies Form? T. M. Takeuchi+ ApJ 2015

Our cosmological zoom-in simulations often produce elongated galaxies like observed ones. The elongated stellar distribution follows the elongated inner dark matter halo.

Prolate DM halo → elongated galaxy

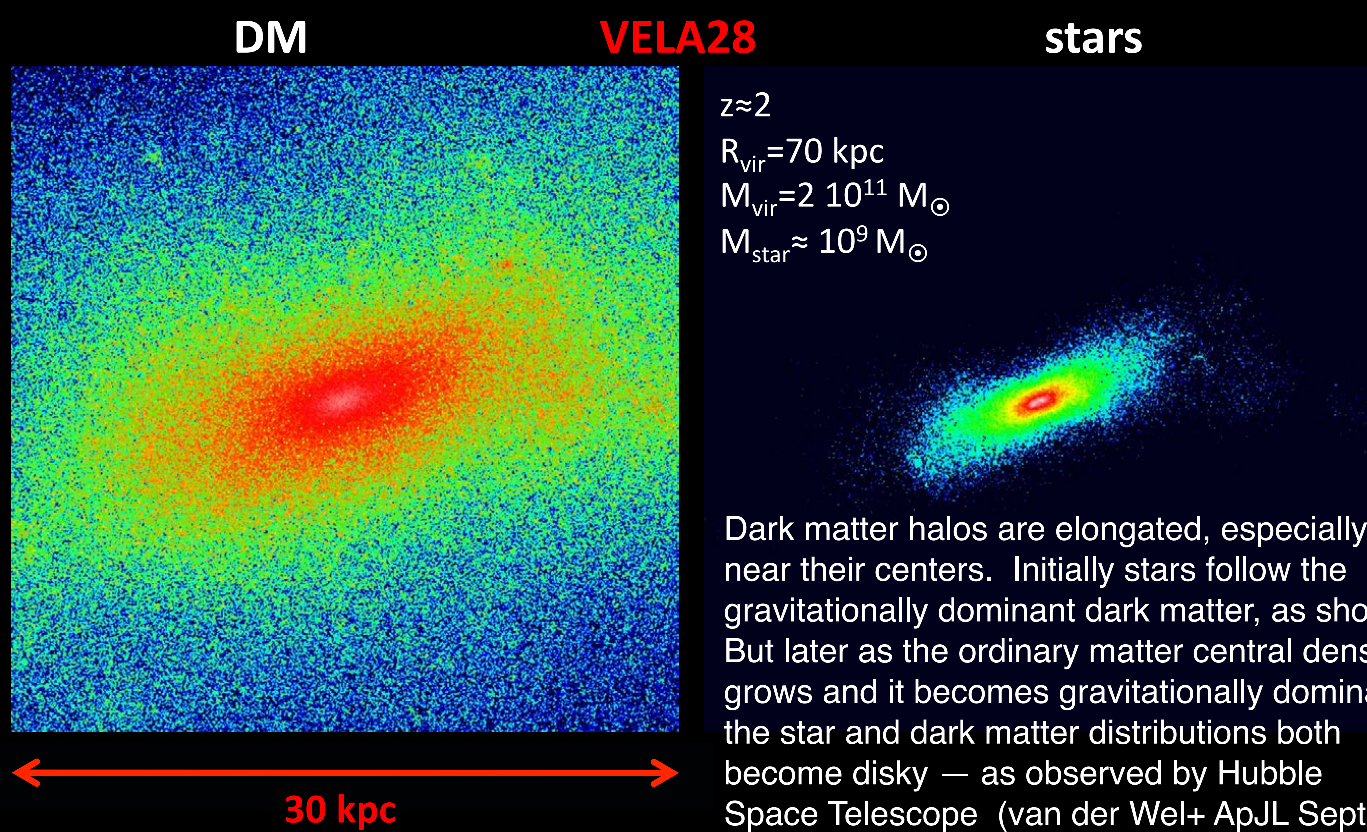

Dark matter halos are elongated, especially near their centers. Initially stars follow the gravitationally dominant dark matter, as shown. But later as the ordinary matter central density grows and it becomes gravitationally dominant, the star and dark matter distributions both become disky — as observed by Hubble Space Telescope (van der Wel+ ApJL Sept 2014).

Monthly Notices of the ROYAL ASTRONOMICAL SOCIETY
MNRAS **453,** 408–413 (2015)

Formation of elongated galaxies with low masses at high redshift

Daniel Ceverino, Joel Primack and Avishai Dekel

ABSTRACT

We report the identification of elongated (triaxial or prolate) galaxies in cosmological simulations at z ~ 2. These are preferentially low-mass galaxies ($M_* \leq 10^{9.5}$ $M_\odot$), residing in dark matter (DM) haloes with strongly elongated inner parts, a common feature of high-redshift DM haloes in the cold dark matter cosmology. A large population of elongated galaxies produces a very asymmetric distribution of projected axis ratios, as observed in high-z galaxy surveys. This indicates that the majority of the galaxies at high redshifts are not discs or spheroids but rather galaxies with elongated morphologies

Nearby large galaxies are mostly disks and spheroids — but they start out looking more like pickles.

Formation of elongated galaxies with low masses at high redshift

Daniel Ceverino, Joel Primack and Avishai Dekel **MNRAS 2015**

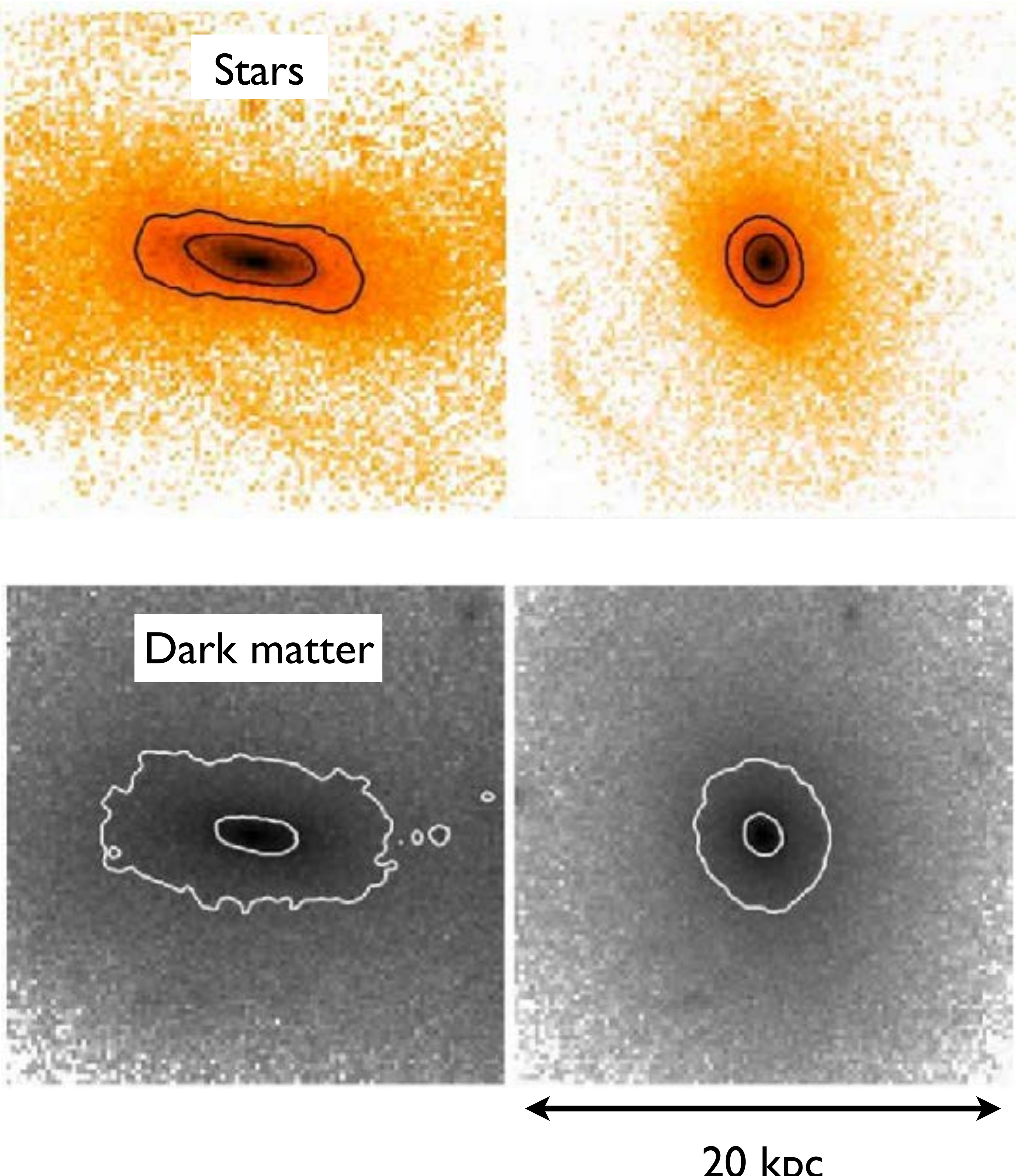

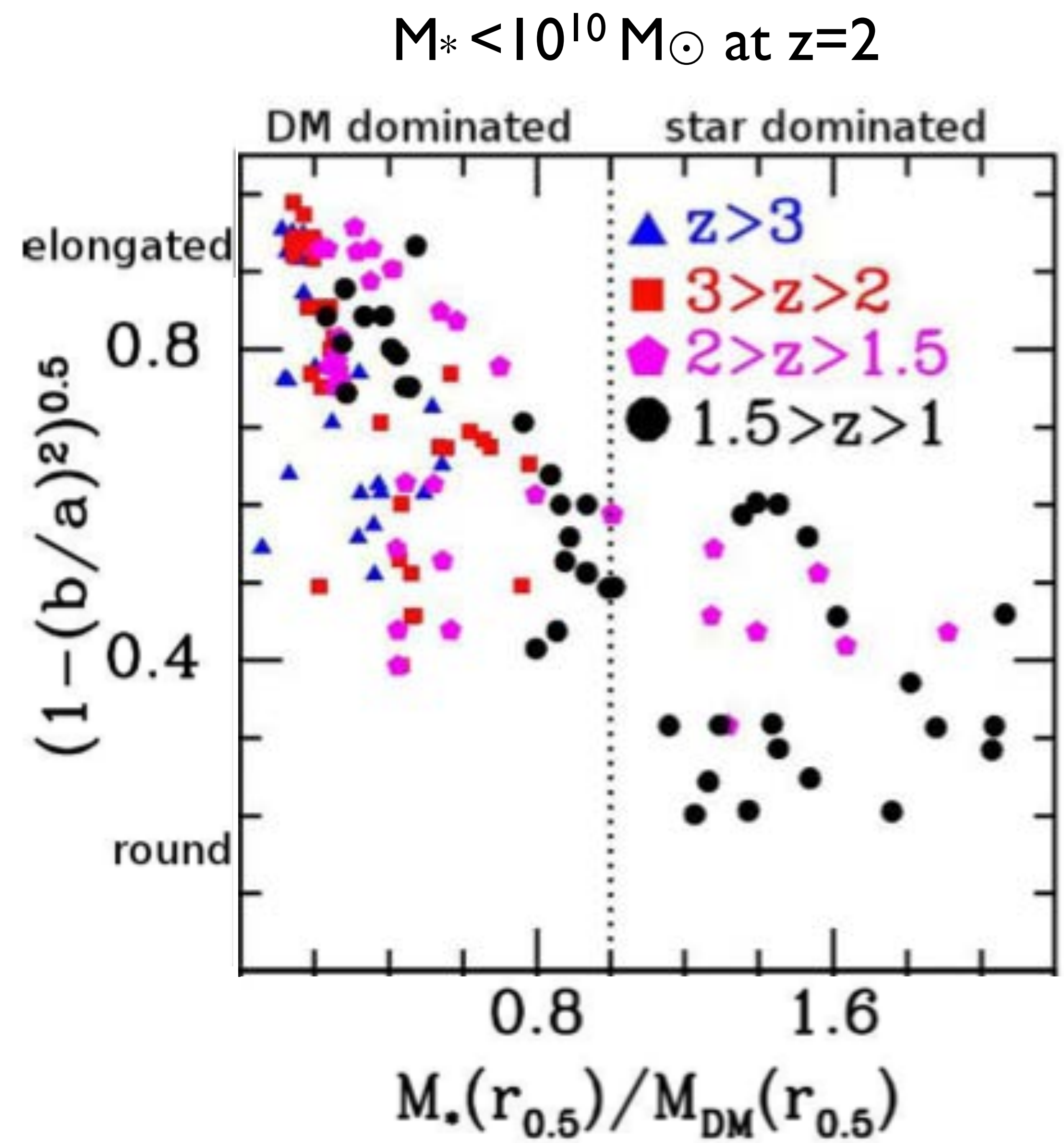

Also Tomassetti et al. 2016 MNRAS

Simulated elongated galaxies are aligned with cosmic web filaments, become round after compaction (gas inflow fueling central starburst)

Kavli Institute for Theoretical Physics
University of California, Santa Barbara

Quantifying and Understanding the Galaxy — Halo Connection

July 7, 2017

Structural Evolution in the Galaxy-Halo Connection, and Halo Properties as a Function of Environment Density and Web Location

Joel Primack

- **Abundance matching with radii & mergers ⇒ $R^* \sim M^{*1/3}$ goes to $R^* \sim M^{*2}$ after quenching, & quenching downsizing: Σ_1 grows till quenching, $\Sigma_{1,quench}$ larger & at higher z for higher M***
- **2-pt Correlation Functions for SHAM with M_{vir} & M_{peak} (OK) and V_{max} & V_{peak} (better)**
- **Halo properties $\dot{M}/M$, λ, C_{NFW}, a_{LMM}, shape don't depend on web location at fixed density**
- **Spin λ 30% smaller at low density tests whether galaxy R* is determined by host halo λ**
- **Halo Mass Loss: Evaporation after Merger ⇒ C_{NFW} ⬇ & λ⬆, Tidal Stripping ⇒ C_{NFW} ⬆ & λ⬇**
- **Galaxy Luminosity-Halo Mass, Stellar Mass-Halo Mass relations are independent of density**
- **Forming galaxies are elongated & oriented along filaments, become round after compaction**